

Accepted Manuscript

Sulfamic acid promoted one-pot synthesis of phenanthrene fused-dihydrodi-benzo-quinolinones: Anticancer activity, tubulin polymerization inhibition and apoptosis inducing studies

Niggula Praveen Kumar, Sowjanya Thatikonda, Ramya Tokala, S. Sujana Kumari, Uppu Jaya Lakshmi, Chandraiah Godugu, Nagula Shankaraiah, Ahmed Kamal

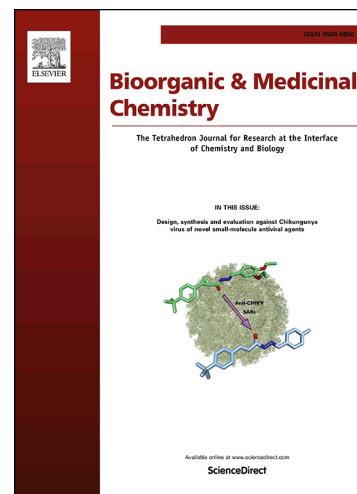
PII: S0968-0896(17)32484-7
DOI: <https://doi.org/10.1016/j.bmc.2018.02.050>
Reference: BMC 14236

To appear in: *Bioorganic & Medicinal Chemistry*

Received Date: 25 December 2017
Revised Date: 21 February 2018
Accepted Date: 28 February 2018

Please cite this article as: Kumar, N.P., Thatikonda, S., Tokala, R., Kumari, S.S., Lakshmi, U.J., Godugu, C., Shankaraiah, N., Kamal, A., Sulfamic acid promoted one-pot synthesis of phenanthrene fused-dihydrodibenzo-quinolinones: Anticancer activity, tubulin polymerization inhibition and apoptosis inducing studies, *Bioorganic & Medicinal Chemistry* (2018), doi: <https://doi.org/10.1016/j.bmc.2018.02.050>

This is a PDF file of an unedited manuscript that has been accepted for publication. As a service to our customers we are providing this early version of the manuscript. The manuscript will undergo copyediting, typesetting, and review of the resulting proof before it is published in its final form. Please note that during the production process errors may be discovered which could affect the content, and all legal disclaimers that apply to the journal pertain.



Sulfamic acid promoted one-pot synthesis of phenanthrene fused-dihydrodibenzo-quinolinones: Anticancer activity, tubulin polymerization inhibition and apoptosis inducing studies

Niggula Praveen Kumar,^a Sowjanya Thatikonda,^c Ramya Tokala,^a S. Sujana Kumari,^b Uppu Jaya Lakshmi,^b Chandraiah Godugu,^{c*} Nagula Shankaraiah,^{a*} Ahmed Kamal^{a*}

^aDepartment of Medicinal Chemistry, ^bDepartment of Pharmacology and Toxicology, ^cDepartment of Regulatory Toxicology, National Institute of Pharmaceutical Education and Research (NIPER), Hyderabad 500 037, India

Abstract

A facile one-pot method for the synthesis of new phenanthrene fused-dihydrodibenzo-quinolinone derivatives has been successfully accomplished by employing sulfamic acid as catalyst. These new compounds were evaluated for their *in vitro* cytotoxic potential against human lung (A549), prostate (PC-3 and DU145), breast (MCF-7) and colon (HT-29 and HCT-116) cancer cell lines. Among all the tested compounds, one of the derivatives **8p** showed good anti-proliferative activity against A549 lung cancer cell line with an IC₅₀ of 3.17 ± 0.52 µM. Flow cytometric analyses revealed that compound **8p** arrested both Sub G1 and G2/M phases of cell cycle in a dose dependent manner. The compound **8p** also displayed significant inhibition of tubulin polymerization and disruption of microtubule network (IC₅₀ of 5.15±0.15 µM). Molecular docking studies revealed that compound **8p** efficiently interacted with critical amino acid Cys241 of the α/β-tubulin by a hydrogen bond (S–H....O = 2.4 Å). Further, the effect of **8p** on cell viability was also studied by AO/EB, DCFDA and DAPI staining. The apoptotic characteristic features revealed that **8p** inhibited cell proliferation effectively through apoptosis by inducing the ROS generation. Analysis of mitochondrial membrane potential through JC-1 staining and annexin V binding assay indicated the extent of apoptosis in A549 cancer cells.

Keywords: Phenanthrene fused-dihydrodibenzo-quinolinones, Perkin condensation, tubulin polymerization, one-pot reaction, apoptosis.

*Corresponding authors: Dr Nagula Shankaraiah, Tel.: (+91) 040 23073740; Fax: (+91) 040 23073751; E-mail: shankar@niperhyd.ac.in; Dr Ahmed Kamal, Tel.: +91-40-27193157; fax: +91-40-27193189; E-mail: ahmedkamal@iict.res.in; Dr. Chandraiah Godugu, E-mail: chandra.niperhyd@gov.in

1.0 Introduction

Cancer has been considered as one of the life threatening diseases worldwide [1]. In spite of tremendous development in the chemotherapeutic drugs, finding efficacious new cytotoxic drugs with minimum off target effects is the active area of research [2]. The principle target for most of the antitumor agents is either apoptosis or cell division [3]. Natural products have been an invaluable source of new chemotherapeutics [4]. *Cyanchum*, *Pergularia*, *Tylophora* and some other genera from the *Asclepiadacea* family serves as natural source for diverse pentacyclic derivatives popularly known as phenanthroindolizidine alkaloids [5]. These nitrogen-containing alkaloids are well distinguished for their broad range of antitumor [6], anti-inflammatory [7], antilupus [8], anti-angiogenic [9], antiarthritis [10], anti-microbial [11], antiviral [12] and antifungal properties [13]. Profound cytotoxic profile of these alkaloids makes them as targets for structure activity modification [14]. Tylophorine was the representative alkaloid of this class, (**Figure 1**) which showed strong growth inhibitory potential on a large number of cancer cells by arresting the cell cycle at G2/M phase [15]. Additionally, these derivatives were also reported to induce apoptosis and inhibit the enzymes involved in the nucleic acid synthesis [16].

On the other hand, podophyllotoxin is a naturally occurring cytotoxic aryl tetralin lignan reported as well-known potent tubulin polymerization inhibitor [17]. Its semi-synthetic derivatives such as etoposide and teniposide are among the frontline chemotherapeutic drugs and are used against various malignancies especially testicular carcinoma, small cell lung cancer, lymphoma and kaposi sarcoma [18]. Further, many research groups have been reported the synthesis of 4-azapodophyllotoxin (**Figure 1**) and its derivatives retaining mitotic phase arrest and anti-tubulin properties comparable to that of podophyllotoxin [19]. In this connection, we rationally designed these new compounds resembling both tylophorine and 4-azapodophyllotoxin in their structures, which may display enhanced cytotoxicity through G2/M phase arrest and apoptosis induction.

Multi-component reactions serve as an effective tool to synthesize diverse range of bioactive molecules by involving minimum number of synthetic steps and improving atom economy [20]. Moreover, in medicinal chemistry point of view, exploring synthetic precursors to obtain biologically active molecules is gaining prominent status [21]. More recently commercially available precursor, 9-amino phenanthroline has been successfully utilized to synthesize phenanthroline based azapodophyllotoxin mimics (**Figure 1**). These derivatives

displayed potent cytotoxicity and tubulin polymerization inhibition properties [22]. Inspired by these significant contributions and in continuation of our earlier efforts dedicated to bioactive podophyllotoxin derivatives, [23] herein, we wish to present a one-pot protocol for the synthesis of modified analogues of azapodophyllotoxin devoid of “D ring”. A new series of phenanthrene fused-dihydrodibenzo-quinolinone derivatives has been synthesized and evaluated for their *in vitro* cytotoxic potential and apoptosis inducing ability. Moreover, we have also explored their tubulin polymerization inhibition capability of these newly synthesized azapodophyllotoxin mimics.

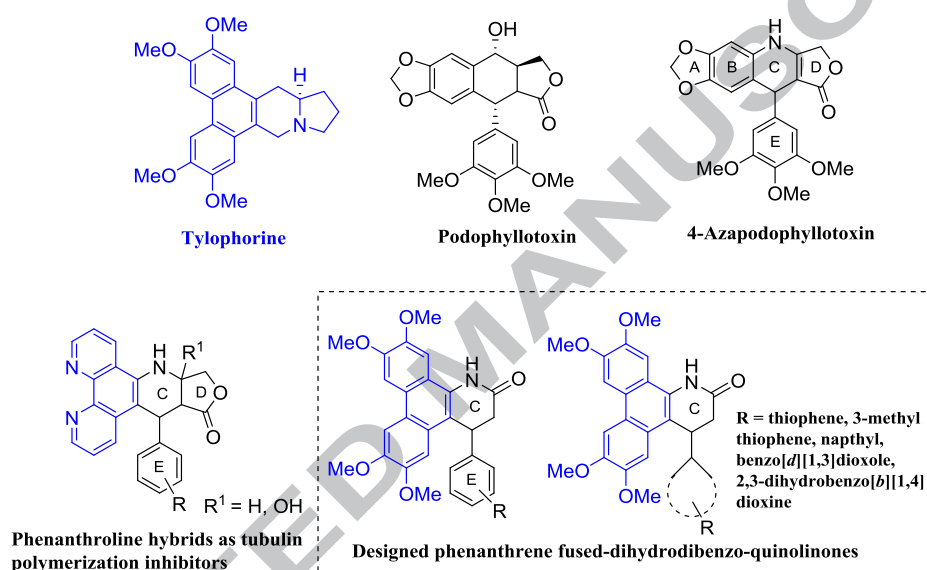


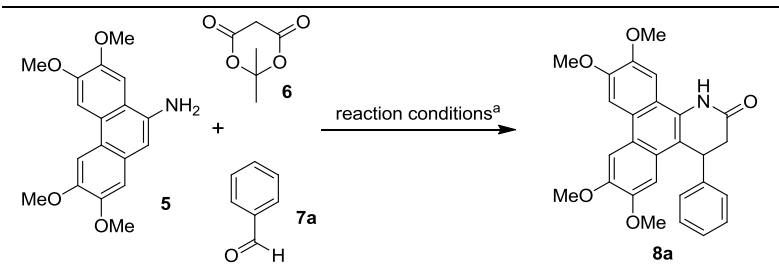
Figure 1. Structures of tylophorine, podophyllotoxin, azapodophyllotoxin derivatives and newly designed phenanthrene fused-dihydrodibenzo-quinolinones.

2.0 Results and discussion

2.1 Chemistry

Phenanthrene fused-dihydrodibenzo-quinolinones **8a–r** were synthesized by a one-pot reaction by using 2,3,6,7-tetramethoxyphenanthren-9-amine (**5**), Meldrums acid (**6**) with various aromatic aldehydes **7a–r** and catalytic amount of sulfamic acid in refluxing ethanol as depicted in **Scheme 1**. Initially, Knoevenagel condensation between Meldrums acid and aldehyde results in the formation of arylidene meldrums acid intermediate followed by the Michael addition of amine and subsequent dehydration, cyclization by loss of CO₂ and acetone affords phenanthrene fused-dihydrodibenzo-quinolinones [24]. Herein, we have also

explored the substrate scope of phenanthrene amine. To our interest, multi-component protocol was optimised by using catalytic amount of sulfamic acid. However, the reaction was also proceeded in absence of Lewis acid, but the yields obtained were not satisfactory. Further to study the feasibility of the reaction, different Lewis acids such as TFA, acetic acid, and bases such as piperidine and Et₃N have been evaluated. Sulfamic acid in ethanol solvent was proved to be the best for this conversion with improved yields (**Table 1**). All the electron-donating, electron-withdrawing, heteroaromatic aldehydes and bicyclic aldehyde participated effectively in the reaction. The key amine precursor **5** was synthesized from benzyl 2,3,6,7-tetramethoxyphenanthren-9-yl carbamate (**4**) in good yield as shown in **Scheme 1**. Compound **4** was prepared from the commercially available starting materials *via* the conventional six step sequence according to the documented procedure [25]. Initially, Perkin condensation of 3,4-dimethoxybenzaldehyde (**2**) and 3,4-dimethoxy phenyl acetic acid (**1**) resulted in the formation of 2,3-bis(3,4-dimethoxyphenyl)acrylic acid. The acid was converted into its methyl ester followed by *m*-CPBA/TFA mediated intramolecular oxidative cyclization [26] to give the tricyclic phenanthrene ester **3**. This ester functionality was converted into acyl hydrazide with hydrazine hydrate followed by diazotization reaction using NaNO₂/HCl-H₂O affords corresponding acyl azide. This acyl azide is converted to 2,3,6,7-tetramethoxyphenanthren-9-yl carbamate (**4**) by Curtius rearrangement. Finally, benzyl-carbamate was deprotected with TBAF to give the tetramethoxy phenanthrene amine (**5**). All the synthesized compounds **8a–r** were characterized by HRMS, ¹H and ¹³C NMR spectroscopy. The ¹H NMR of compound **8a** showed a sharp singlet at δ 9.83 ppm representing the typical NH proton. The two signals, multiplet at 3.34 ppm and doublet at 2.99 corresponds to -CH₂- of the amido hexocyclic C ring. Proton attached to tertiary carbon is detected as doublet at δ 4.90 ppm. Characteristic methoxy protons appeared as a singlet of three protons around δ 3.29–4.13 ppm. In ¹³C NMR spectrum of compound **8a** the carbonyl carbon appeared at δ 170.8 ppm. The methoxy substituted carbons resonated around δ 148.1–149.5 ppm. The signal attributed to the -CH₂- of the C ring appeared at δ 39.3 ppm. Tertiary carbon showed a characteristic peak of δ 39.2 ppm and all the aromatic carbons resonates around δ 101.7–141.3 ppm. Similar pattern was observed in ¹H NMR and ¹³C NMR of all the final compounds **8b–r**. The HRMS (ESI) of all the derivatives showed an [M + H]⁺ peak equivalent to their corresponding molecular formula.

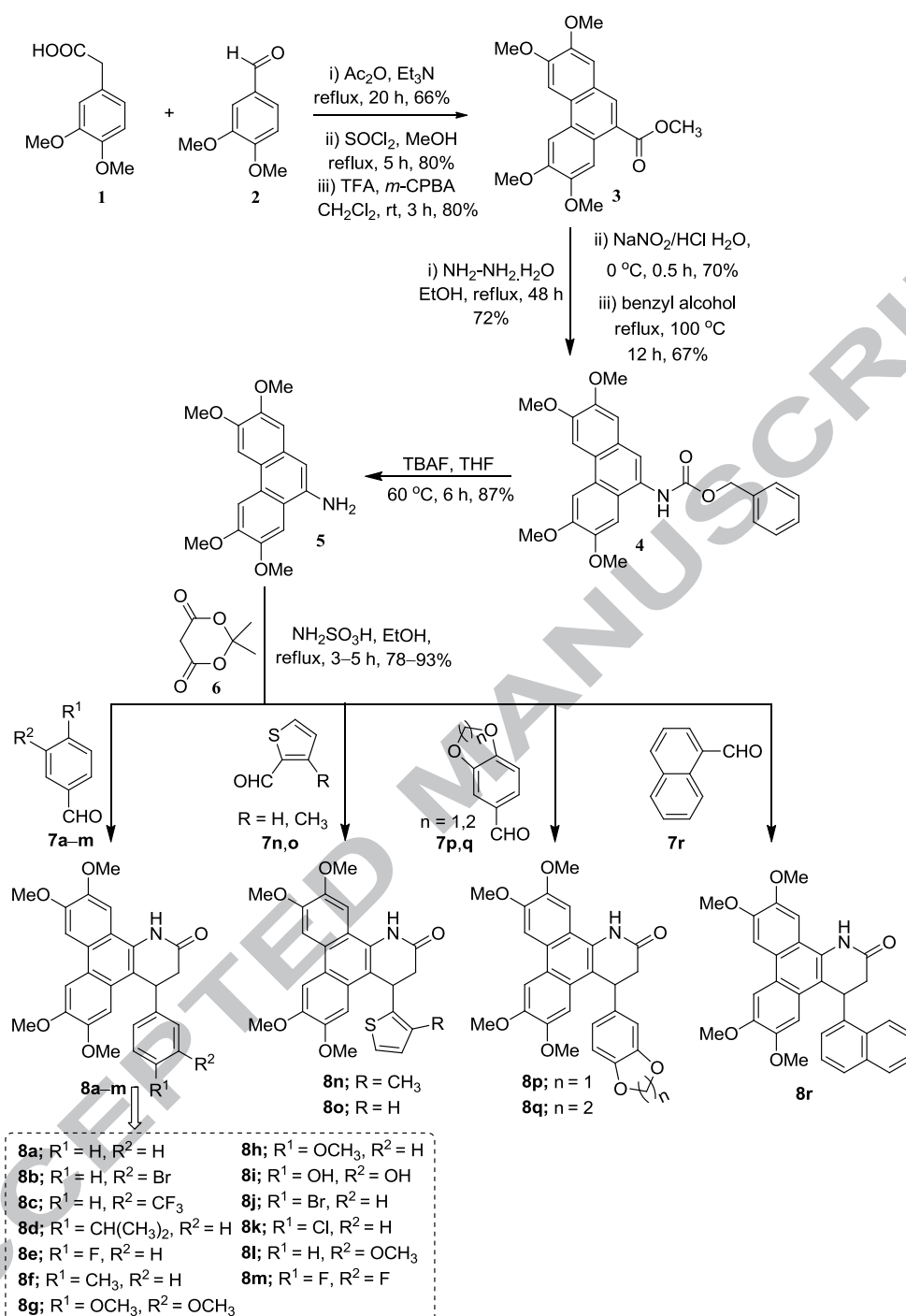
Table 1. Optimization of the reaction conditions^a for the one-pot synthesis of **8a**


The reaction scheme shows the one-pot synthesis of compound **8a** from three starting materials: **5** (3,4,5-trimethoxyaniline), **6** (3,4-dihydro-2H-pyran-2-one), and **7a** (benzaldehyde). The reaction proceeds under conditions ^a to yield **8a** (3,4,5-trimethoxy-N-phenyl-1,2,3,4-tetrahydroquinolin-2(1H)-one).

entry	reagent	solvent	temperature (°C)	time (h)	yield (%) ^b
1	-	EtOH	80	3	57
2	-	EtOH	80	12	59
3	TFA	EtOH	80	12	61
4	TFA	EtOH	80	12	54
5	Et ₃ N	EtOH	80	12	68
6	piperidine	EtOH	80	12	72
7	NH₂SO₃H	EtOH	80	3	89
8	NH ₂ SO ₃ H	H ₂ O	60	12	-

^aReaction conditions: **5** (0.22 mmol), **6** (0.22 mmol), **7** (0.22 mmol), catalyst or base (20 mol%) and solvent (3 mL) .

^bIsolated yields.



Scheme 1. One-pot synthesis of new phenanthrene fused-dihydrodibenzo-quinolinones (**8a-r**).

2.2 Biology

2.2.1 *In vitro* cytotoxic activity

The newly synthesized phenanthrene fused-dihydrodibenzo-quinolinones **8a-r** were screened for their *in vitro* cytotoxicity against different human cancer cell lines such as lung (A549),

prostate (PC-3 and DU145), breast (MCF-7) and colon (HT 29 and HCT-116) by using 3-(4,5-dimethylthiazol-2-yl)-2,5-diphenyltetrazolium bromide (MTT) assay [27]. The IC_{50} (μM) values (concentration required to inhibit 50% of the cancer cells) of the tested compounds and the standard drugs etoposide and podophyllotoxin are listed in **Table 2**. It is observed from the initial screening that derivatives **8e** and **8p** displayed broad range of activity against all the tested cancer cell lines with an IC_{50} values ranging from $3.17 \pm 0.52 \mu M$ to $19.89 \pm 0.21 \mu M$ (**Table 2**). Compound **8p** with 3,4-methylenedioxy substitution on aromatic E ring was found to be most active on all the cancer cell lines particularly on A549 cancer cells (IC_{50} $3.17 \pm 0.52 \mu M$). With close analysis of IC_{50} data, it was observed that most of the compounds were not adequately active against MCF7 (breast cancer) cells except **8e** and **8p** with an IC_{50} values of 12.23 ± 0.51 and $9.59 \pm 0.16 \mu M$, respectively. All the compounds (except **8a**, **8b**, **8f**, **8i**, **8l**, **8n** and **8r**) displayed significant activity less than $10 \mu M$ on A549 (lung cancer) cells with **8p** being the most potent (IC_{50} $3.17 \pm 0.52 \mu M$) followed by derivative **8g** (IC_{50} $4.09 \pm 0.48 \mu M$) with a 3,4- dimethoxy substitution on E ring. Majority of the tested compounds (except **8i**, **8j**, **8m**, **8o** and **8q**) were active against DU145 prostate cancer cell line, with derivative **8c** possessing trifluoromethyl substitution on E ring being the most active (IC_{50} $6.19 \pm 0.09 \mu M$). Derivatives such as **8c**, **8e**, **8h**, **8i**, **8p** and **8q**, were found to be active on PC-3 prostate cancer cell line, while rest of them were inactive on this particular cell line at $20 \mu M$. Compound **8o** with a heterocyclic thiophene E ring showed cytotoxicity on three of the tested cancer cells with an IC_{50} values between 8.50 ± 0.11 and $18.94 \pm 0.32 \mu M$. However, **8n** with a methyl thiophene substitution was active only on DU145 (prostate) and A549 (lung) cancer cell lines. Most of the compounds (except **8a**, **8b**, **8f**, **8l**, **8n** and **8q**) were active against the two tested colon cancer cell lines. The most active compound against these cell lines **8p** followed by **8g** bearing the 3,4-dimethoxy substitution (HCT-116, IC_{50} value: $8.12 \pm 0.04 \mu M$). It could be observed from the *in vitro* cytotoxicity studies that derivatives containing 3,4-disubstitution and oxygen hetero atom in their E ring such as methylenedioxy (**8p**), 3,4-dimethoxy (**8g**) and 3,4-dihydroxy (**8i**) showed improved biological response. On the other hand, fluorine substituted analogues such as **8c** (3-trifluoromethyl) and **8e** (4-fluoro) were also displayed remarkable activity on lung (A549) and prostate (DU145) cancer cells. Moreover, sulphur containing heterocyclic E ring was also displayed improved cytotoxicity as the compound **8o** with a thiophene ring displayed IC_{50} value of $8.50 \pm 0.11 \mu M$ on A549 lung cancer cells. Based on the cytotoxicity results, the most active compounds **8p** was taken-up for further studies towards the mechanism of cancer cell growth inhibition and tubulin polymerization inhibition.

Table 2. *In vitro* cytotoxic activity (IC₅₀ in μ M)^a of phenanthrene fused-dihydrodibenzo quinolinones **8a–r**

Compound	PC-3 ^b	DUI45 ^c	MCF7 ^d	A549 ^e	HT29 ^f	HCT-116 ^g
8a	>20	18.84±0.12	>20	>20	>20	>20
8b	>20	18.49±0.27	>20	>20	>20	>20
8c	18.49±0.27	6.19±0.09	>20	5.03±0.09	18.71±0.13	15.42±0.05
8d	>20	18.2±0.02	>20	8.84±0.03	16.01±0.09	>20
8e	19.89±0.21	11.1±0.1	12.23±0.51	6.29±0.09	17.4±0.10	16.2±0.1
8f	>20	16.92±0.08	>20	16.71±0.06	>20	>20
8g	>20	13.12±0.02	>20	4.09±0.48	12.21±0.04	8.12±0.04
8h	19.09±0.06	17.02±0.07	>20	8.94±0.32	16.71±0.13	>20
8i	19.79±0.12	>20	>20	11.58±0.05	10.3±0.04	12.6±0.14
8j	>20	>20	>20	7.16±0.18	15.54±0.10	16.5±0.12
8k	>20	19.0±0.11	>20	6.49±0.09	13.78±0.08	14.2±0.3
8l	>20	18.91±0.21	>20	>20	>20	>20
8m	>20	>20	>20	7.78±0.08	17.85±0.12	13.4±0.21
8n	>20	19.59±0.08	>20	15.4±0.25	>20	>20
8o	>20	>20	>20	8.50±0.11	18.94±0.32	13.8±0.45
8p	12.11±0.03	17.51±0.17	9.59±0.16	3.17±0.52	7.84±0.03	7.61±0.21
8q	18.40±0.06	>20	>20	7.95±0.31	>20	>20
8r	-	16.1±0.17	>20	14.69±0.39	18.37±0.20	17.16±0.1
Etoposide ^h	5.4±0.2	2.13±0.13	2.03±0.05	3.25±0.09	1.8±0.1	2.6±0.07
Podophyllotoxin ⁱ	0.07±0.003	0.063±0.008	-	0.09±0.009	-	-

^a50% inhibitory concentration after 48 h of compound treatment; ^{b,c}prostate cancer cells; ^dbreast cancer cells; ^elung cancer cells; ^{f,g}Colon cancer cells; ^hEtoposide: positive control; ⁱpodophyllotoxin: reference drug.

2.2.2 Apoptosis induction studies

a. DAPI nuclear staining

DAPI (4',6-diamidino-2-phenylindole) is a fluorescent stain that rigidly binds to A-T rich sequence of nucleic acid and reveals the nuclear damage through chromatin condensation. DAPI penetrates the intact cell membrane with less efficiency when compared to disintegrated cell membrane. Therefore, intensity of stained live cells is less in comparison to apoptotic cells. Apoptotic features such as condensed nuclei make them to stain brighter. Hence, it is of great importance to know the effect of compound **8p** on A549 cells by using DAPI staining [28]. Moreover, this nuclear morphology technique differentiates the live cells from apoptotic cells. DAPI forms fluorescent complex with chromatin there by stains the nucleus bright blue. As observed from **Figure 2**, the nuclear structure of control cells was intact, whereas compound **8p** treated A549 cells showed condensed and horse-shoe shaped nuclei indicating the extent of apoptosis.

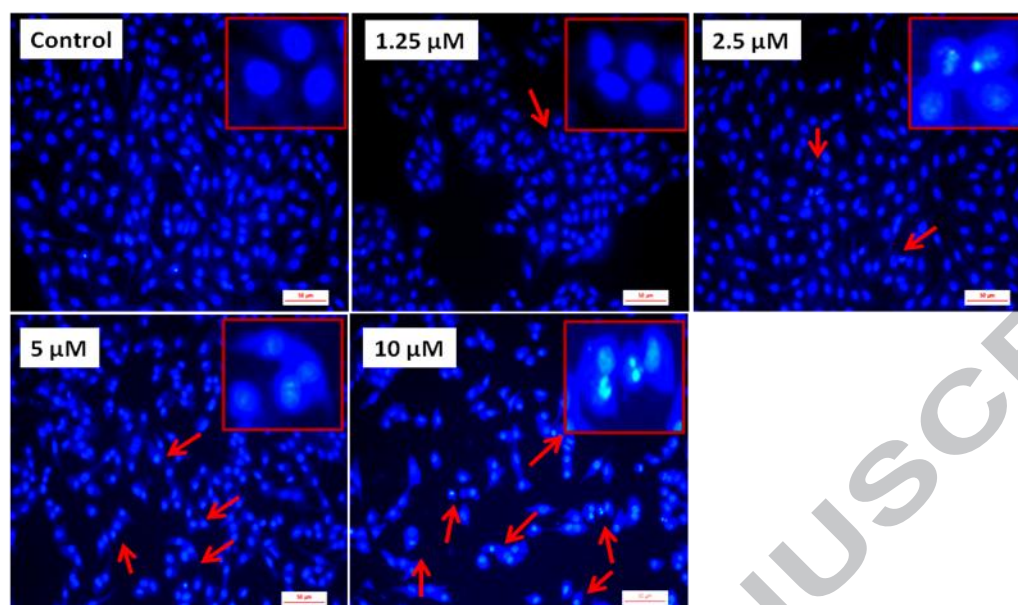


Figure 2. Nuclear morphology in A549 cells stained with DAPI. A549 cancer cells treated with compound **8p** and stained with DAPI. The images were taken with fluorescence microscope with a DAPI filter.

b. Acridine orange–ethidium bromide (AO–EB) staining

Live cells, apoptotic and necrotic cells can be differentiated by performing Acridine orange/ethidium bromide (AO/EB) fluorescent staining assay [29]. AO readily diffuses the normal cell membrane and stains the nuclei green, whereas EB penetrates only membrane disintegrated cells and smear the nucleus in red. In **Figure 3** green colour of the control cells is due to their normal morphology. Fluorescence microscopic images of cells treated with 10.0 μM of compound **8p** clearly shows the altered morphological characteristics such as cell shrinkage, chromatin condensation, membrane blebbing and apoptotic body formation, suggesting that the compound **8p** induced cell death in A549 lung tumor cells.

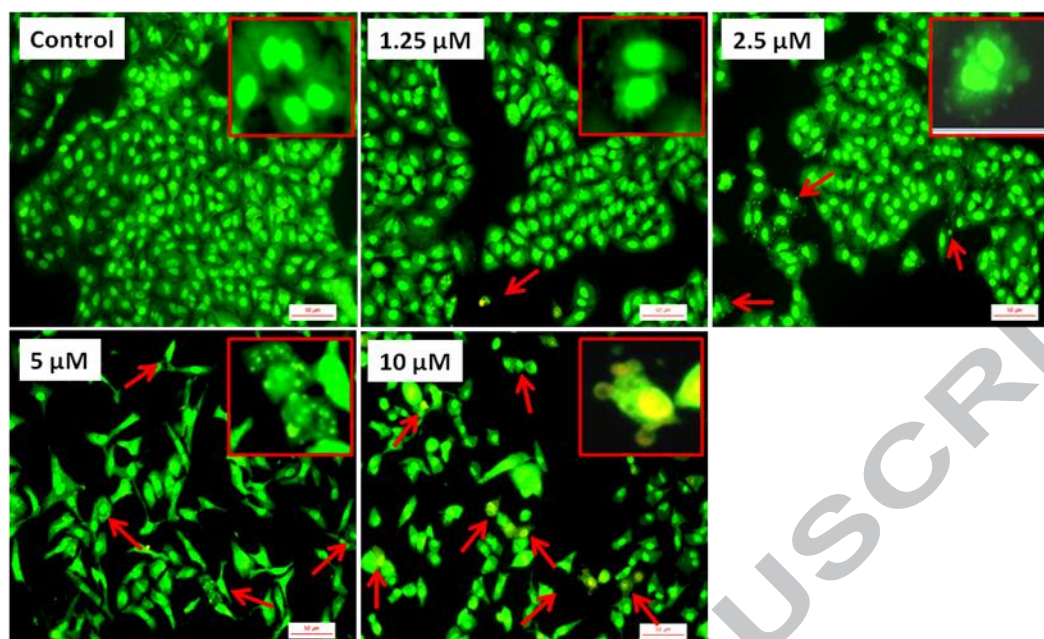


Figure 3. A549 cells were treated with increased concentrations of compound **8p** and stained with AO/EB. Decreased number of viable cells and apoptotic characteristics were observed at 200X magnification.

c. Morphological studies

Microscopic observation could reveal the effect of compounds on cell viability. A549 cancer cells were treated with 1.25, 2.5, 5.0 and 10.0 μM concentrations of active compound **8p**. Cells were observed for morphological alterations and images were captured by using phase contrast microscope. It is clearly observed from **Figure 4**, as the concentration of the compound increases there is a clear decrease in cell viability with significant morphological changes such as cell shrinkage and detachment were observed. This indicates the compound induced distinctive morphological changes in A549 lung cancer cells.

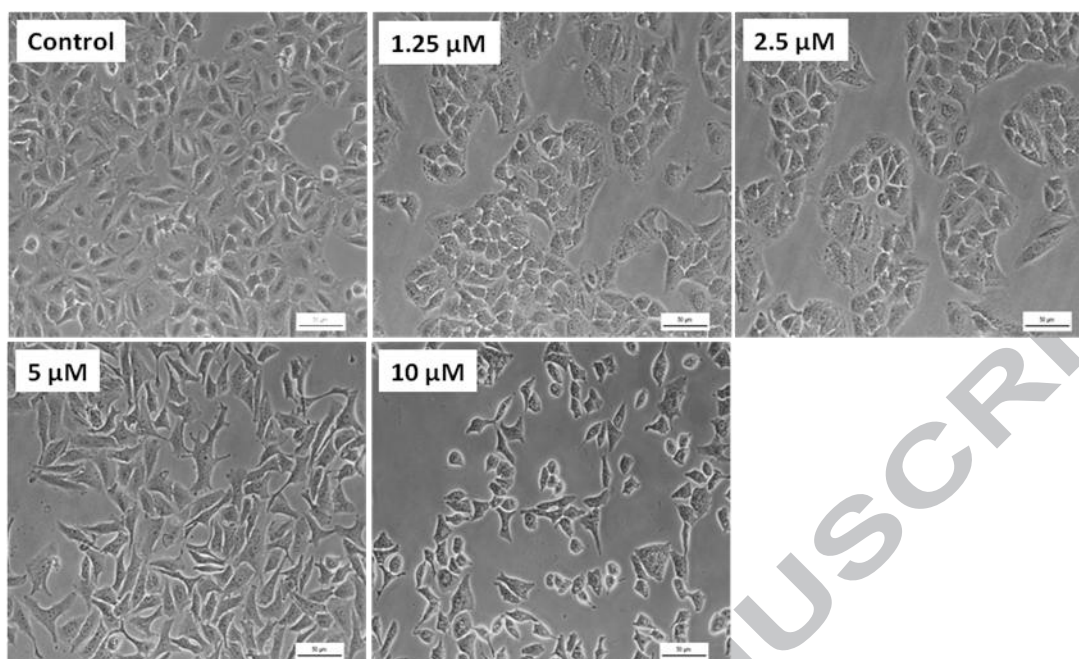


Figure 4. Phase contrast imaging: A549 cells were treated with different concentrations of compound **8p** and observed for their morphological changes at 200X magnification.

d. Effect of compound 8p on reactive oxygen species (ROS)

Most of the cytotoxic compounds induce apoptosis by the generation of ROS, where it initiates oxidative damage to the mitochondrial membrane potential and permeability. Hence, to assess the extent of ROS generation by compound **8p** in A549 cells, DCFDA staining method [30] was performed. A549 cells were treated with compound **8p** resulted in enhanced DCFDA fluorescence in a dose dependent manner, indicating the capability of compound in accumulating ROS (**Figure 5**). Whereas decrease in fluorescence intensity was observed in case of N-acetyl cysteine (NAC) treated A549 cells, thus indicating the decreased free radical production by NAC, which suggest one of the mechanism of cytotoxicity is by elevating ROS levels. On the other hand, increased fluorescence was observed with the positive control H_2O_2 due to the generation of radicals.

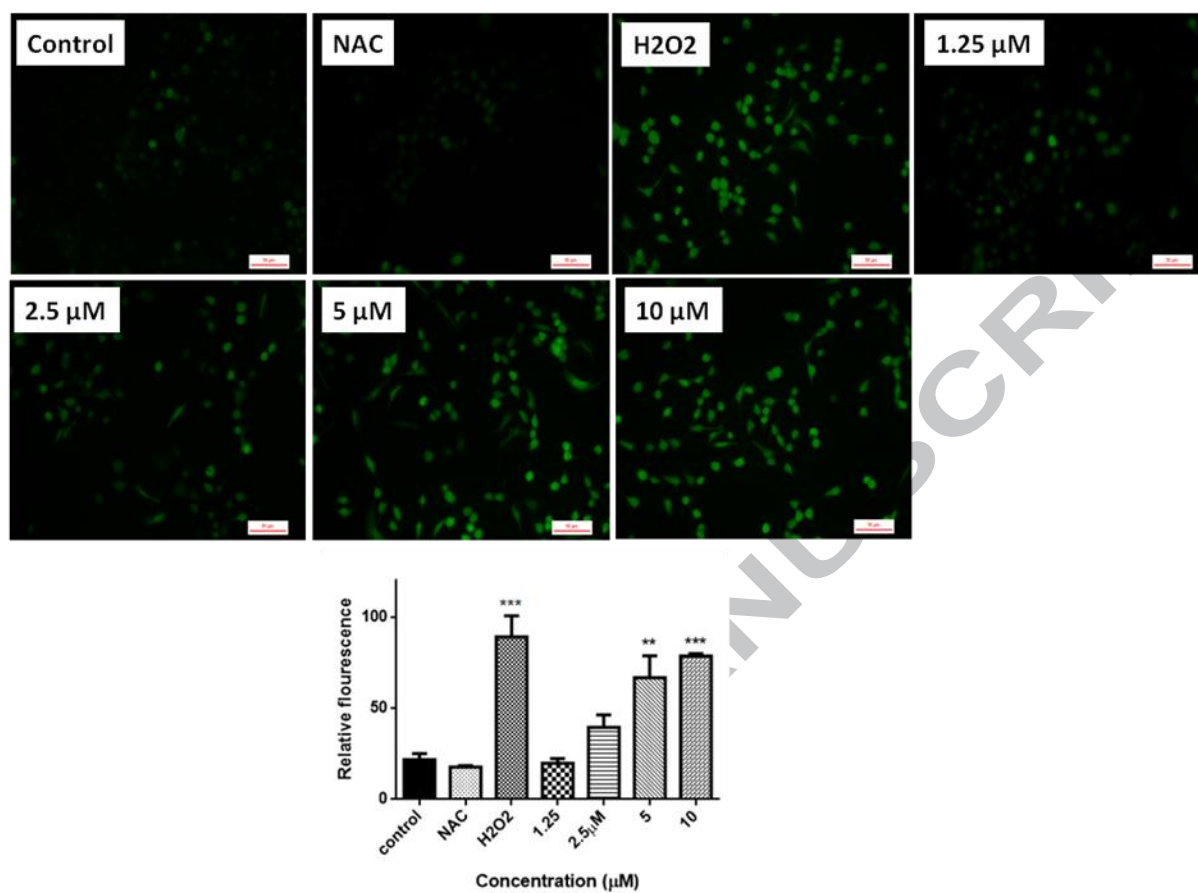
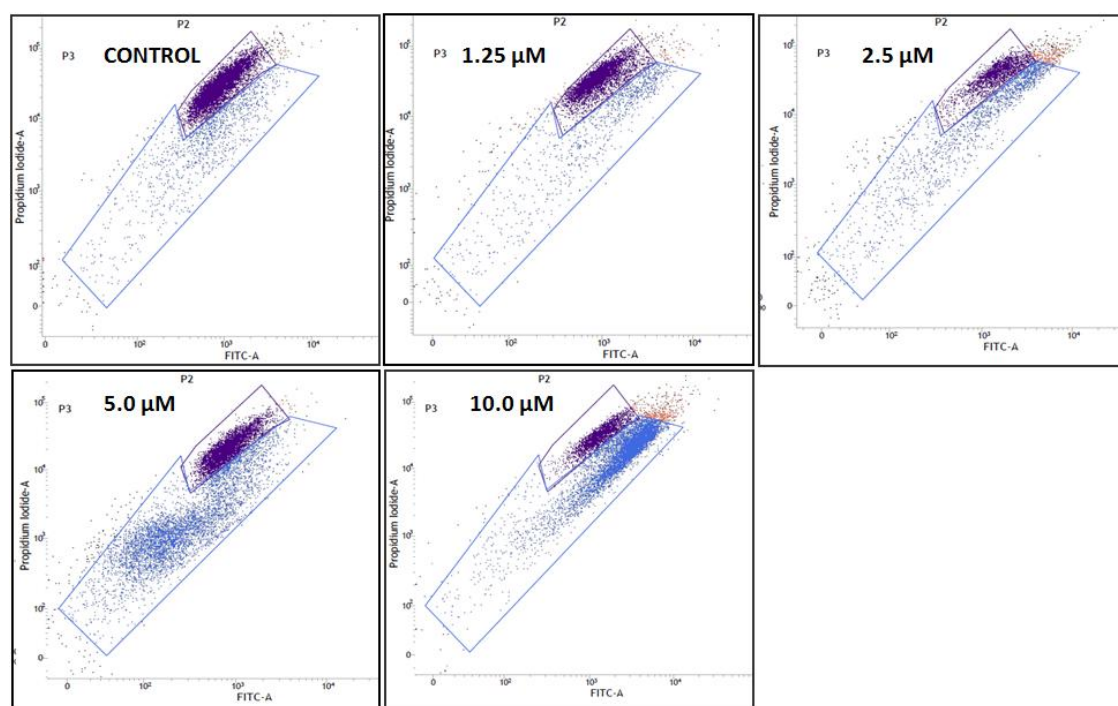


Figure 5. Effect of compound **8p** on Reactive Oxygen Species (ROS) levels. Dose dependent increment of fluorescence observed compared to control. Data presented as mean \pm SEM (n=3). ** $P < 0.01$ and *** $P < 0.001$ versus control.

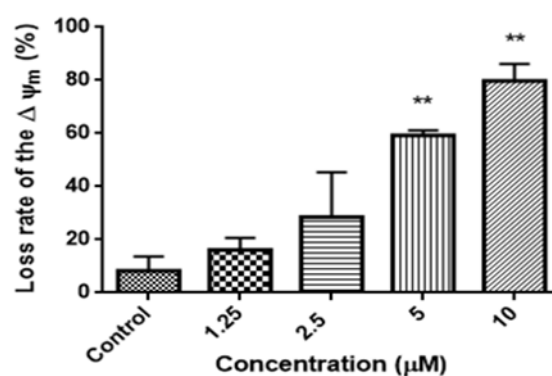
d. Analysis of mitochondrial membrane potential ($\Delta\Psi_m$)

Increased ROS generation could lead to oxidative stress thereby causes alterations in mitochondrial membrane potential. Therefore, it is considered of interest to observe the effect of compound **8p** on mitochondrial membrane potential ($\Delta\Psi_m$). JC-1, a lipophilic cationic dye was used to stain the mitochondria [31]. Normal polarised mitochondria stains in red due to formation of J-aggregates, whereas depolarised mitochondria of apoptotic cells stains in green because of J-monomers. A549 cells were treated with 1.25, 2.5, 5.0 and 10.0 μM of compound **8p** for 24 h and stained with JC-1 dye. Flow cytometric analysis showed increase in depolarised cell population (P3) from control 8.31 ± 3.72 to $79.80 \pm 4.54\%$ at 10.0 μM in

concentration dependent manner (**Figure 6**). Thus, the results indicate decreased mitochondrial membrane potential ($\Delta\Psi_m$) in A549 cells.



A



B

Figure 6 (A and B). Effect of **8p** on mitochondrial membrane potential ($\Delta\Psi_m$). A549 cells were treated with 1.25, 2.5, 5.0 and 10.0 μM of **8p**, incubated with JC-1 stain and analysed by flow cytometer (BD FACSVerseTM, USA). Data presented as mean \pm SEM (n=3). ** $P<0.01$ versus control.

e. AnnexinV /Propidium iodide dual staining assay

Annexin V/propidium iodide dual staining assay was performed to determine the extent of apoptosis induced by the compound **8p** on A549 cells. This assay facilitates the detection of necrotic cells (Q1-NC; AV-/PI+), live cells (Q2-LC; AV-/PI-), late apoptotic cells (Q3- LA; AV+/PI+), and early apoptotic cells (Q4- EA; AV+/PI-). As observed from **Figure 7**, the percentage of total apoptotic cells (early and late apoptotic cells) increased to 52.53% after treatment with 10 μ M concentration of **8p**, in comparison to the control (5.98%) cells. The percentage of early and late apoptotic cells comparatively increased with an increase in the concentration of compound **8p**, which indicates the induction of dose dependent apoptosis in A549 cancer cells.

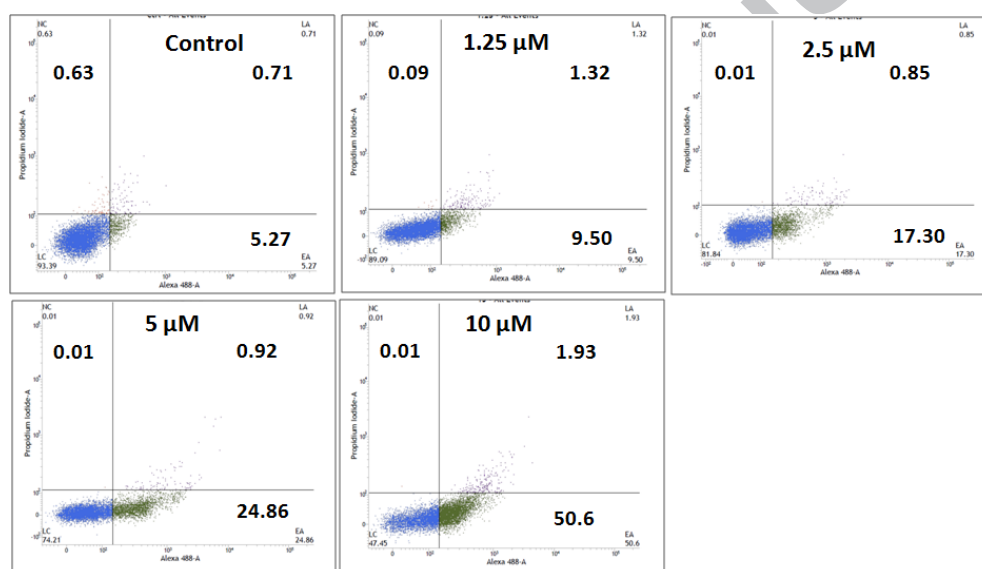


Figure 7. Annexin binding assay for the detection of apoptosis. The compound **8p** treated cells were stained with Annexin V/PI and analysed for apoptosis. 10,000 cells from each sample were analysed by flowcytometry. The percentage of cells positive for Annexin V/Propidium iodide is represented inside the quadrants.

2.2.3 Cell cycle analysis

Arresting specific phase of the cell cycle is the characteristic feature of most of the cytotoxic compounds. Thus blockade of cell cycle progression by cytotoxic agents has a vital role to develop effective chemotherapeutic agents. From *in vitro* screening data, it was observed that the compound **8p** displayed significant cytotoxic potential against A549 lung cancer cells.

Therefore, we studied the effect of compound **8p** on distribution of cell population in each phases of cell cycle by flow cytometry analysis [32]. A549 cells were treated with compound **8p** at 1.25, 2.5, 5.0 and 10.0 μM for 48 h, and the cells were fixed using ethanol, stained with propidium iodide and analyzed by flow cytometry. The results from **Figure 8** shows that the compound **8p** arrested A549 cells in G2/M phase from $34.25 \pm 5.75\%$ (control) to $61.20 \pm 3.32\%$ (10.0 μM), In addition, significant Sub G1 phase arrest is also observed in concentration dependant manner from $4.52 \pm 2.47\%$ in control to $31.22 \pm 4.03\%$ at 10.0 μM .

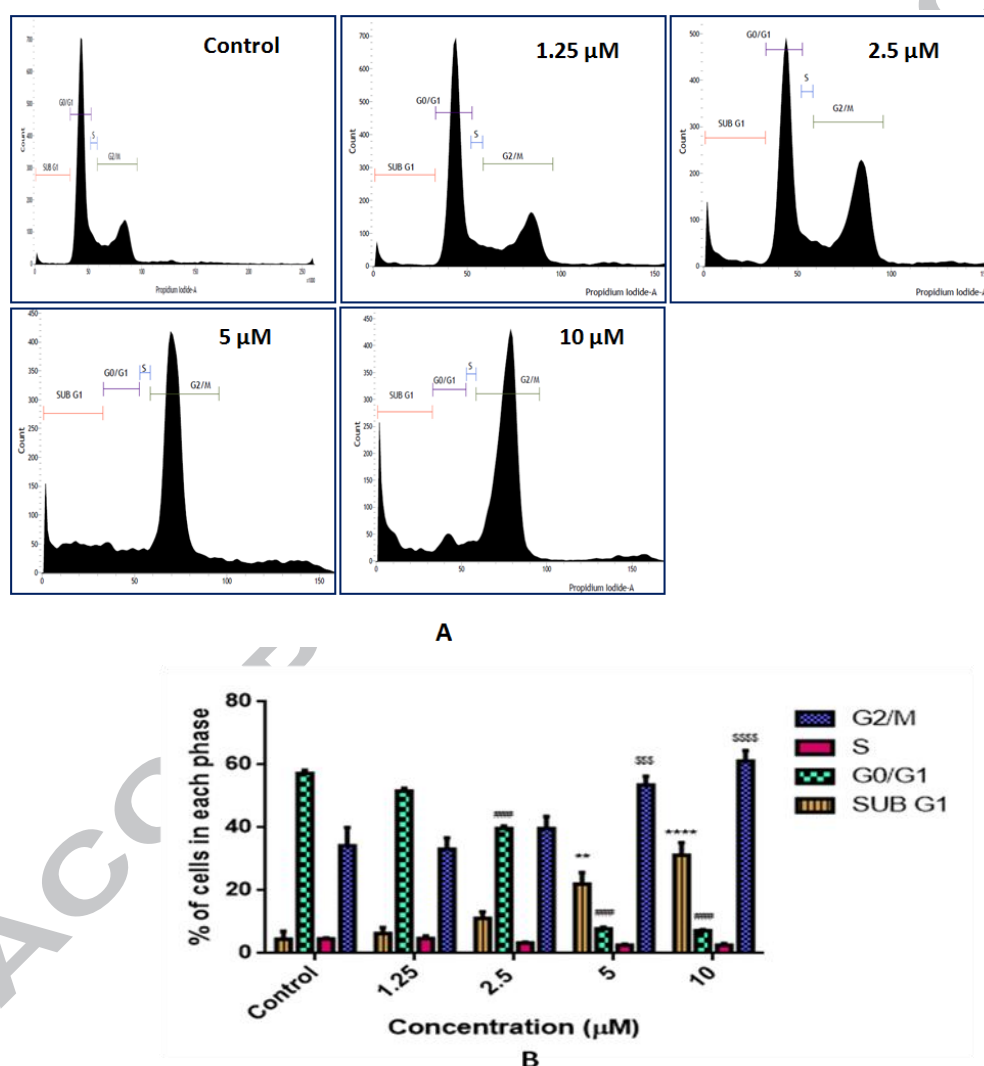


Figure 8 (A and B). Cell cycle analysis of A549 lung cancer cells treated with **8p** for 48 h. The cell cycle distribution was analysed by flow cytometry using propidium iodide staining method. Data presented as mean \pm SEM (n=3). ** $P < 0.01$ and **** $P < 0.0001$ versus control Sub G1 population; ##### $P < 0.0001$ versus control G0/G1 population; \$\$\$ $P < 0.001$ and \$\$\$\$ $P < 0.0001$ versus control G2/M population.

2.2.4 Effect on tubulin polymerization

As these new compounds have structural resemblance to the podophyllotoxin, it was considered of pertinent to know their effect on microtubule system. The compound **8p** was investigated for its tubulin polymerization inhibitory potential in a cell-free *in vitro* assay [33]. The inhibition of tubulin assembly is most of the times associated with G2/M cell cycle arrest in most of the cancer cells. The compound **8p** also displayed G2/M cell cycle arrest. Hence, we studied the ability of compound **8p** to inhibit tubulin polymerization by monitoring the increase in fluorescence emission at 440 nm (excitation wavelength is 360 nm) for 1 h at 37 °C (**Figure 9**). In this study, podophyllotoxin and paclitaxel, were used as reference standards at 5 μ M and 3 μ M concentrations respectively. Compound **8p** was used at final concentrations of 10, 5, 2.5, 1.25 μ M respectively. The experiment was performed in duplicates. The IC₅₀ value was calculated from the drug concentration required to inhibit 50% of tubulin assembly compared to control. Interestingly, the compound **8p** displayed potent tubulin polymerization inhibition with an IC₅₀ value of 5.15 \pm 0.15 μ M.

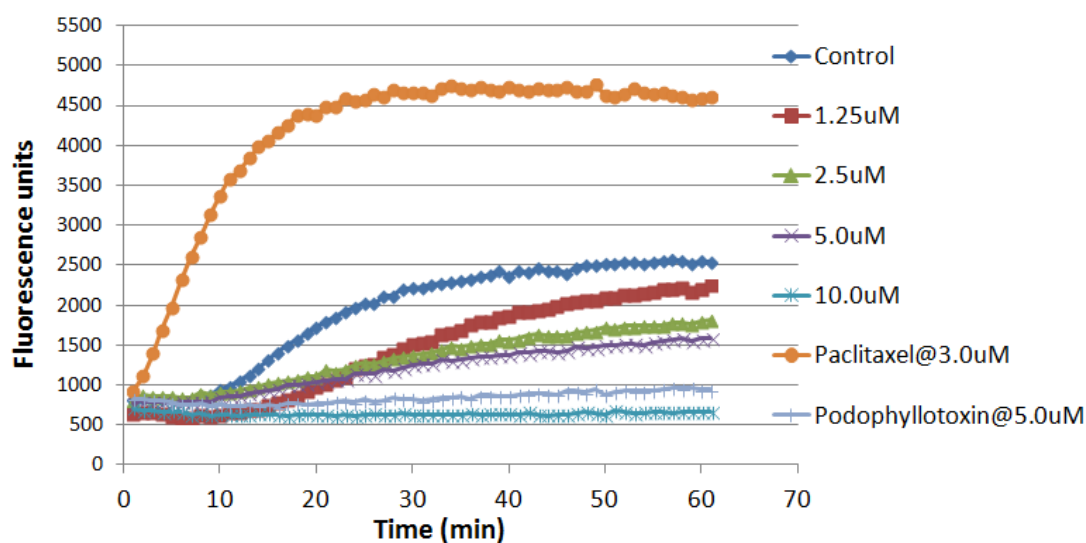


Figure 9. Effect of compound **8p** on the tubulin polymerization: tubulin polymerization was monitored by the increase in fluorescence at 360 nm (excitation) and 440 nm (emission) for 1 h at 37 °C.

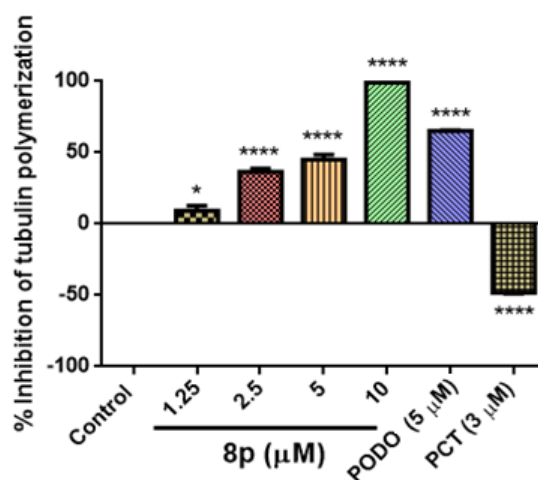


Figure 10. % Dose-response inhibition of tubulin polymerization by compound **8p** at final concentrations of 10, 5, 2.5, 1.25 μ M. Podophyllotoxin and paclitaxel, were used as reference standards. Data expressed as mean \pm SEM (n=3). * P <0.05 and **** P <0.0001 versus control.

2.2.5 Molecular docking

To understand the mode of binding with tubulin, active compound **8p** was docked into the podophyllotoxin binding site of α/β -tubulin (PDB ID: 1SA1) located at the interface of the α,β subunits [34]. Co-crystallized ligand podophyllotoxin was re-docked into tubulin so as to compare the interaction pattern. The podophyllotoxin interacted strongly with the critical amino acid residues Cys241 and Leu252 in the binding site of tubulin. The interaction with Cys241 is attributed due to the hydrogen-bonding with oxygen atom corresponding to the trimethoxy 'E' ring of the podophyllotoxin. Therefore, this amino acid residue is critical and has important role in binding to modified podophyllotoxin derivatives retaining 'E' ring in their structure. Interestingly, compound **8p** displayed strong hydrogen-bond interactions with Cys241, Lys254, Asn258, and Gln11 amino acid residues of the binding site (**Figure 11**). Oxygen of methylene dioxy 'E' ring of the compound **8p** interacted strongly with critical amino acid Cys241 by a hydrogen-bond (S–H.....O = 2.4 Å). Compound **8p** also exhibited strong hydrophobic interactions with Val177, Ala180, Tyr224, Cys241, Leu248, Ala250, Ala316, Ala317, Val318 and Ala354. Moreover, the oxygen atom of amide carbonyl corresponding to hexocyclic 'C' ring formed a hydrogen-bonding with the side chain of Asn258 (N–H.....O = 2.6 Å). Additionally, the two oxygen atoms of the methoxy groups substituted on the planar phenanthrene system formed hydrogen-bonding with side chain of Lys254 (N–H.....O = 1.8 Å) and Gln11 (N–H.....O = 3.4 Å). Cys241 played a crucial role during the protein-ligand binding process, possibly explaining the stronger inhibitory activity

of compound **8p**. All these binding modes were responsible to the hypothesis that these new azapodophyllotoxin derivatives exhibit efficient binding in to the podophyllotoxin binding site on tubulin and thus displaying antitubulin activity.

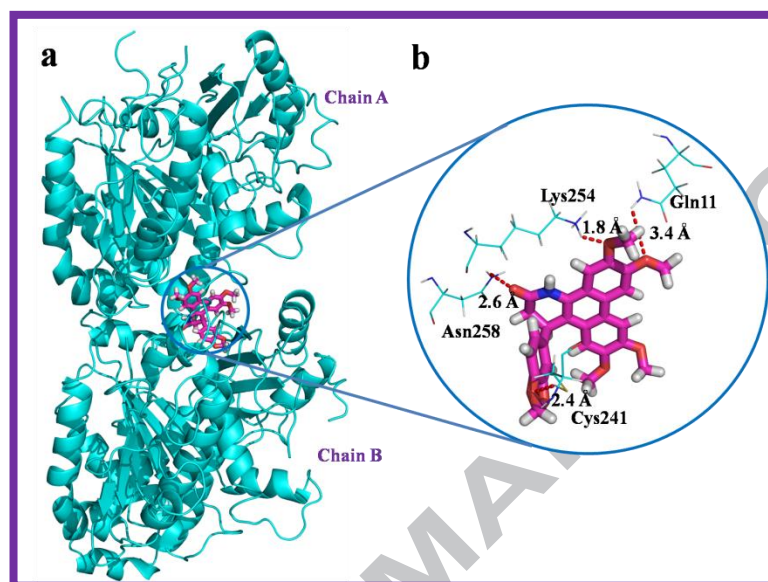


Figure 11. a) Docking model of the most potent compound **8p** (magenta colour stick) and b) its ligand-protein interactions in the podophyllotoxin binding site of α/β -tubulin (PDB ID: 1SA1). The red dashed lines represent hydrogen bonds.

3.0 Conclusion

In conclusion, a new series of phenanthrene fused-dihydrodibenzo-quinolinone derivatives were synthesized and evaluated for their *in vitro* cytotoxic potential against various selected human cancer cell lines. From the initial screening, it was observed that some of the derivatives were active on most of the tested cancer cell lines with IC_{50} values below 20 μ M. The *in vitro* screening results indicated that most active compound **8p** showed broad range of activity on all the tested cell lines with a significant IC_{50} value of 3.17 ± 0.52 μ M on A549 lung cancer cells. The cell cycle analysis indicated that it blocked both Sub G1 and G2/M phase of the cell cycle. Moreover, the compound also decreased viable cells by inducing apoptotic changes as shown in case of AO/EB and DAPI staining. JC-1 and Annexin-V/PI staining revealed the dose dependent apoptosis induction by **8p** in lung cancer cells with elevated ROS generation. Further, compound **8p** effectively led to the inhibition of tubulin

polymerization by increasing the concentrations. Molecular docking studies also supported the possible mode of binding to the α/β -tubulin. Overall, the current study indicates that these new azapodophyllotoxin mimics have the potential to be advanced as microtubule targeting cytotoxic agents for the treatment of cancer.

4.0 Experimental protocols

4.1 Chemistry

All reagents and solvents were obtained from commercial suppliers and were used without further purification. Analytical thin layer chromatography (TLC) was performed on MERCK precoated silica gel 60-F₂₅₄ (0.5 mm) aluminum plates. Visualization of the spots on TLC plates was achieved by UV light. ¹H and ¹³C NMR spectra were recorded on Bruker 500 MHz making a solution of samples in CDCl₃ solvent using tetramethyl silane (TMS) as the internal standard. Chemical shifts for ¹H and ¹³C are reported in parts per million (ppm) downfield from tetra methyl silane. Spin multiplicities are described as s (singlet), bs (broad singlet), d (doublet), t (triplet), q (quartet), and m (multiplet). Coupling constant (*J*) values are reported in hertz (Hz). HRMS were determined with Agilent QTOF mass spectrometer 6540 series instrument. Wherever required, column chromatography was performed using silica gel (60-120 or 100-200) or neutral alumina. The reactions wherever anhydrous conditions required are carried under nitrogen positive pressure using freshly distilled solvents. All evaporation of solvents was carried out under reduced pressure on Heidolph rotary evaporator below 45 °C.

4.1.1 General reaction procedure for the synthesis of phenanthrene fused-dihydrodibenzo-quinolin-ones **8a–r**

A mixture of 2,3,6,7-tetramethoxy phenanthrene-9-amine (**5**, 0.22 mmol), Meldrums acid (**6**, 0.22 mmol) and substituted aldehydes (**7a–r**, 0.22 mmol), and sulfamic acid (20 mol%) in EtOH (3 mL) was refluxed for 3–5 h. After the completion of the reaction, the reaction mixture was allowed to cool to room temperature and the precipitated products was collected by vacuum filtration and washed with water and followed by recrystallization from ethanol to afford pure compounds **8a–r** in 78-93% yields. All the synthesized compounds were thoroughly characterized by ¹H NMR, ¹³C NMR and HRMS (ESI).

4.1.1.1 6,7,10,11-Tetramethoxy-4-phenyl-3,4-dihydrodibenzo[f,h]quinolin-2(1H)-one (**8a**)

Light brown solid, yield 89%; mp: >300 °C; ¹H NMR (500 MHz, CDCl₃): δ 9.83 (s, 1H), 7.84 (s, 1H), 7.79 (s, 1H), 7.51 (s, 1H), 7.22 (t, *J* = 8.24 Hz, 2H), 7.16 (t, *J* = 7.32 Hz, 4H), 4.90 (d, *J* = 7.01 Hz, 1H), 4.13 (s, 3H), 4.08 (s, 3H), 3.99 (s, 3H), 3.85 (s, 3H), 3.34–3.29 (m, 1H), 2.99 (d, *J* = 15.71 Hz, 1H) ppm; ¹³C NMR (125 MHz, CDCl₃): δ 170.8, 149.5, 149.4, 149.3, 148.1, 141.3, 129.3, 129.0 (2C), 127.1, 127.0 (2C), 124.9, 124.3, 122.0, 117.3, 114.7, 104.1, 103.6, 103.5, 101.7, 56.2, 56.1 (2C), 55.6, 39.3, 39.2 ppm; HRMS (ESI): *m/z* calcd for C₂₇H₂₅NO₅ 444.1805, found 444.1808 [M+H]⁺.

4.1.1.2 4-(3-Bromophenyl)-6,7,10,11-tetramethoxy-3,4-dihydrodibenzo[*f,h*]quinolin-2(1*H*)-one (8*b*)

Light brown solid, yield 92%; mp: 271–273 °C; ¹H NMR (500 MHz, CDCl₃): δ 9.70 (s, 1H), 7.83 (s, 1H), 7.79 (s, 1H), 7.48 (s, 1H), 7.34–7.30 (m, 2H), 7.10–7.08 (m, 3H), 4.86 (d, *J* = 7.32 Hz, 1H), 4.13 (s, 3H), 4.09 (s, 3H), 4.01 (s, 3H), 3.87 (s, 3H), 3.33–3.29 (m, 1H), 2.96 (d, *J* = 15.86 Hz, 1H) ppm; ¹³C NMR (125 MHz, CDCl₃): δ 170.4, 149.6, 149.5, 149.4, 148.2, 143.8, 130.6, 130.4, 130.1, 129.5, 125.7, 125.0, 124.1, 123.1, 122.0, 117.2, 113.7, 103.8, 103.7, 103.4, 101.8, 56.2, 56.1, 56.0, 55.7, 39.2, 38.8 ppm; HRMS (ESI): *m/z* calcd for C₂₇H₂₄BrNO₅ 522.0911, found 522.0904 [M+H]⁺.

4.1.1.3 6,7,10,11-Tetramethoxy-4-(3-(trifluoromethyl)phenyl)-3,4-dihydrodibenzo[*f,h*]quinolin-2(1*H*)-one (8*c*)

Off white solid, yield 90%; mp: 290–292 °C; ¹H NMR (500 MHz, CDCl₃): δ 9.77 (s, 1H), 7.84 (s, 1H), 7.80 (s, 1H), 7.56 (s, 1H), 7.51 (s, 1H), 7.47 (d, *J* = 7.47 Hz, 1H), 7.32–7.27 (m, 2H), 7.07 (s, 1H), 4.95 (d, *J* = 7.32 Hz, 1H), 4.14 (s, 3H), 4.08 (s, 3H), 4.00 (s, 3H), 3.85 (s, 3H), 3.38–3.33 (m, 1H), 2.98 (d, *J* = 15.71 Hz, 1H) ppm; ¹³C NMR (125 MHz, CDCl₃): δ 170.3, 149.6, 149.5, 149.4, 148.2, 142.6, 131.4 (d, *J*_{C-F} = 31.7 Hz), 130.4, 129.7, 129.6, 125.1, 124.9 (d, *J*_{C-F} = 272.4 Hz), 124.1 (d, *J*_{C-F} = 3.6 Hz), 124.0, 123.9, 122.0, 117.2, 113.6, 103.7 (2C), 103.5, 101.9, 56.1 (3C), 55.6, 39.1, 39.0 ppm; HRMS (ESI): *m/z* calcd for C₂₈H₂₄F₃NO₅ 512.1679, found 512.1680 [M+H]⁺.

4.1.1.4 4-(4-Isopropylphenyl)-6,7,10,11-tetramethoxy-3,4-dihydrodibenzo[*f,h*]quinolin-2(1*H*)-one (8*d*)

Off white solid, yield 89%; mp: 295–297 °C; ¹H NMR (500 MHz, CDCl₃): δ 9.85 (s, 1H), 7.83 (s, 1H), 7.78 (s, 1H), 7.53 (s, 1H), 7.19 (s, 1H), 7.08 (dd, *J* = 8.24, 21.66 Hz, 4H), 4.86

(d, $J = 7.17$ Hz, 1H), 4.13 (s, 3H), 4.08 (s, 3H), 3.99 (s, 3H), 3.87 (s, 3H), 3.31–3.26 (m, 1H), 2.97 (d, $J = 15.71$ Hz, 1H), 2.81–2.75 (m, 1H), 1.15 (d, $J = 6.86$ Hz, 6H) ppm; ^{13}C NMR (125 MHz, CDCl_3): δ 171.2, 149.4, 149.3, 149.2, 147.9, 147.5, 138.7, 129.3, 127.0 (2C), 126.8 (2C), 124.7, 124.4, 121.9, 117.4, 115.0, 104.2, 103.5, 103.3, 102.0, 56.2, 56.1, 56.0, 55.6, 39.3, 38.8, 33.5, 23.8 (2C) ppm; HRMS (ESI): m/z calcd for $\text{C}_{30}\text{H}_{31}\text{NO}_5$ 486.2275, found 486.2274 $[\text{M}+\text{H}]^+$.

4.1.1.5 4-(4-Fluorophenyl)-6,7,10,11-tetramethoxy-3,4-dihydrodibenzo[*f,h*]quinolin-2(1H)-one (8e)

Light brown solid, yield 90%; mp: >300 °C; ^1H NMR (500 MHz, CDCl_3): δ 9.82 (s, 1H), 7.83 (s, 1H), 7.79 (s, 1H), 7.51 (s, 1H), 7.13–7.09 (m, 3H), 6.88 (t, $J = 8.54$ Hz, 2H), 4.88 (d, $J = 7.17$ Hz, 1H), 4.13 (s, 3H), 4.08 (s, 3H), 4.01 (s, 3H), 3.85 (s, 3H), 3.38–3.32 (m, 1H), 2.94 (d, $J = 15.71$ Hz, 1H) ppm; ^{13}C NMR (125 MHz, CDCl_3): δ 170.7, 162.7, 160.8, 149.5, 149.4, 149.3, 148.1, 137.0, 136.9 (d, $J_{\text{C-F}} = 3.6$ Hz), 129.4, 128.6 (d, $J_{\text{C-F}} = 8.1$ Hz), 124.9, 124.1 (d, $J_{\text{C-F}} = 236.1$ Hz), 117.3, 115.9, 115.7, 114.4, 103.8, 103.6, 103.4, 101.9, 56.2, 56.1, 56.0, 55.6, 39.4, 38.4 ppm; HRMS (ESI): m/z calcd for $\text{C}_{27}\text{H}_{24}\text{FNO}_5$ 462.1711, found 462.1714 $[\text{M}+\text{H}]^+$.

4.1.1.6 6,7,10,11-Tetramethoxy-4-(*p*-tolyl)-3,4-dihydrodibenzo[*f,h*]quinolin-2(1H)-one (8f)

Off white solid, yield 93%; mp: >300 °C; ^1H NMR (500 MHz, CDCl_3): δ 9.93 (s, 1H), 7.83 (s, 1H), 7.78 (s, 1H), 7.55–7.53 (m, 1H), 7.16 (s, 1H), 7.06–6.99 (m, 4H), 4.85 (d, $J = 7.17$ Hz, 1H), 4.13 (s, 3H), 4.07 (s, 3H), 3.98 (s, 3H), 3.86 (s, 3H), 3.26–3.13 (m, 1H), 2.95 (d, $J = 15.56$ Hz, 1H), 2.23 (s, 3H) ppm; ^{13}C NMR (125 MHz, CDCl_3): δ 171.1, 149.4, 149.3, 149.2, 147.9, 138.3, 136.6, 129.6 (2C), 129.4, 126.8 (2C), 124.7, 124.4, 121.9, 117.4, 114.9, 104.0, 103.4, 103.3, 102.0, 56.2, 56.1, 56.0, 55.6, 39.4, 38.4, 20.9 ppm; HRMS (ESI): m/z calcd for $\text{C}_{28}\text{H}_{27}\text{NO}_5$ 458.1962, found 458.1964 $[\text{M}+\text{H}]^+$.

4.1.1.7 4-(3,4-Dimethoxyphenyl)-6,7,10,11-tetramethoxy-3,4-dihydrodibenzo[*f,h*]quinolin-2(1H)-one (8g)

White solid, yield 87%; mp: 229–230 °C; ^1H NMR (500 MHz, CDCl_3): δ 9.86 (s, 1H), 7.84 (s, 1H), 7.79 (s, 1H), 7.53 (s, 1H), 7.17 (s, 1H), 6.77 (s, 1H), 6.66–6.62 (m, 2H), 4.84 (d, $J = 6.86$ Hz, 1H), 4.14 (s, 3H), 4.08 (s, 3H), 4.02 (s, 3H), 3.87 (s, 3H), 3.75 (s, 3H), 3.72 (s, 3H), 3.30–3.25 (m, 1H), 2.98 (d, $J = 15.56$ Hz, 1H) ppm; ^{13}C NMR (125 MHz, CDCl_3): δ 171.1,

149.4, 149.3, 149.2, 149.1, 148.1, 148.0, 133.8, 129.3, 124.8, 124.3, 121.9, 119.1, 117.3, 115.0, 111.4, 110.3, 104.0, 103.5, 103.4, 101.9, 56.1, 56.0 (2C), 55.8, 55.7, 55.6, 39.4, 38.8 ppm; HRMS (ESI): m/z calcd for $C_{29}H_{29}NO_7$ 504.2017, found 504.2012 $[M+H]^+$.

4.1.1.8 6,7,10,11-Tetramethoxy-4-(4-methoxyphenyl)-3,4-dihydrodibenzo[*f,h*]quinolin-2(1*H*)-one (8*h*)

Yellow solid, yield 81%; mp: 297–299 °C; 1H NMR (500 MHz, $CDCl_3$): δ 9.86 (s, 1H), 7.83 (s, 1H), 7.78 (s, 1H), 7.52 (s, 1H), 7.15 (s, 1H), 7.08 (d, $J = 8.08$ Hz, 2H), 6.74 (d, $J = 8.24$ Hz, 2H), 4.84 (d, $J = 6.40$ Hz, 1H), 4.13 (s, 3H), 4.08 (s, 3H), 4.00 (s, 3H), 3.86 (s, 3H), 3.68 (s, 3H), 3.29–3.25 (m, 1H), 2.95 (d, $J = 15.56$ Hz, 1H) ppm; ^{13}C NMR (125 MHz, $CDCl_3$): δ 170.9, 158.5, 149.5, 149.4, 149.3, 148.0, 133.2, 129.2, 128.0 (2C), 124.8, 124.3, 121.9, 117.3, 115.1, 114.3, 114.1, 104.1, 103.5, 103.4, 101.7, 56.2, 56.1, 56.0, 55.6, 55.1, 39.5, 38.4 ppm; HRMS (ESI): m/z calcd for $C_{28}H_{27}NO_6$ 474.1911, found 474.1914 $[M+H]^+$.

4.1.1.9 4-(3,4-Dihydroxyphenyl)-6,7,10,11-tetramethoxy-3,4-dihydrodibenzo[*f,h*]quinolin-2(1*H*)-one (8*i*)

Light brown solid, yield 81%; mp: >300 °C; 1H NMR (500 MHz, $DMSO-d_6$): δ 10.35 (s, 1H), 8.52 (Br, s, 2H), 7.92 (s, 1H), 7.87 (s, 1H), 7.75 (s, 1H), 7.16 (s, 1H), 6.61 (d, $J = 8.08$ Hz, 1H), 6.54 (d, $J = 8.08$ Hz, 1H), 6.47 (s, 1H), 4.74 (d, $J = 7.17$ Hz, 1H), 4.04 (s, 3H), 3.99 (d, $J = 3.05$ Hz, 6H), 3.77 (s, 3H), 3.10–3.06 (m, 1H), 2.67 (d, $J = 15.41$ Hz, 1H) ppm; ^{13}C NMR (125 MHz, $CDCl_3+DMSO-d_6$): δ 169.4, 148.7, 148.5, 148.4, 147.3, 144.8, 143.7, 132.9, 129.6, 124.1, 124.0, 121.0, 117.7, 117.1, 115.4, 114.7, 114.0, 104.0, 103.8, 103.6, 103.5, 102.8, 55.8, 55.7, 55.6, 55.0, 37.6 ppm; HRMS (ESI): m/z calcd for $C_{27}H_{25}NO_7$ 476.1704, found 476.1710 $[M+H]^+$.

4.1.1.10 4-(4-Bromophenyl)-6,7,10,11-tetramethoxy-3,4-dihydrodibenzo[*f,h*]quinolin-2(1*H*)-one (8*j*)

White solid, yield 88%; mp: >300 °C; 1H NMR (500 MHz, $CDCl_3$): δ 10.03 (s, 1H), 7.83 (s, 1H), 7.79 (s, 1H), 7.53 (s, 1H), 7.33 (d, $J = 8.54$ Hz, 2H), 7.07 (s, 1H), 7.04 (d, $J = 8.39$ Hz, 2H), 4.86 (d, $J = 7.17$ Hz, 1H), 4.13 (s, 3H), 4.08 (s, 3H), 4.02 (s, 3H), 3.85 (s, 3H), 3.34–3.30 (m, 1H), 2.95 (d, $J = 15.71$ Hz, 1H) ppm; ^{13}C NMR (125 MHz, $CDCl_3$): δ 170.6, 149.5, 149.4 (2C), 148.1, 140.3, 132.1 (2C), 129.5, 128.8 (2C), 124.9, 124.0, 122.0, 121.0, 117.2, 114.0, 103.7, 103.6, 103.4, 101.9, 56.2, 56.1, 56.0, 55.6, 39.1, 38.6 ppm; HRMS (ESI): m/z calcd for $C_{27}H_{24}BrNO_5$ 522.0911, found 522.0904 $[M+H]^+$.

4.1.1.11 4-(4-Chlorophenyl)-6,7,10,11-tetramethoxy-3,4-dihydrodibenzo[f,h]quinolin-2(1H)-one (8k)

Off white solid, yield 86%; mp: >300 °C; ¹H NMR (500 MHz, CDCl₃): δ 9.85 (s, 1H), 7.84 (s, 1H), 7.79 (s, 1H), 7.50 (s, 1H), 7.18 (d, *J* = 8.54 Hz, 2H), 7.09 (d, *J* = 9.46 Hz, 3H), 4.87 (d, *J* = 7.01 Hz, 1H), 4.13 (s, 3H), 4.08 (s, 3H), 4.02 (s, 3H), 3.85 (s, 3H), 3.33–3.29 (m, 1H), 2.96 (d, *J* = 15.71 Hz, 1H) ppm; ¹³C NMR (125 MHz, CDCl₃): δ 170.7, 149.5, 149.4, 149.3, 148.1, 139.7, 132.9, 129.4, 129.1 (2C), 128.4 (2C), 124.9, 124.0, 122.0, 117.2, 114.0, 103.8, 103.6, 103.4, 102.0, 56.2, 56.1, 56.0, 55.6, 39.2, 38.5 ppm; HRMS (ESI): *m/z* calcd for C₂₇H₂₄ClNO₅ 478.1416, found 478.1419 [M+H]⁺.

4.1.1.12 6,7,10,11-Tetramethoxy-4-(3-methoxyphenyl)-3,4-dihydrodibenzo[f,h]quinolin-2(1H)-one (8l)

Yellow solid, yield 85%; mp: 288–290 °C; ¹H NMR (500 MHz, CDCl₃): δ 9.44 (s, 1H), 7.83 (s, 1H), 7.78 (s, 1H), 7.42 (s, 1H), 7.15 (t, *J* = 7.32 Hz, 2H), 6.78 (d, *J* = 7.62 Hz, 1H), 6.71 (d, *J* = 7.78 Hz, 2H), 4.86 (d, *J* = 7.01 Hz, 1H), 4.13 (s, 3H), 4.08 (s, 3H), 4.01 (s, 3H), 3.86 (s, 3H), 3.66 (s, 3H), 3.30–3.26 (m, 1H), 2.99 (d, *J* = 15.8 Hz, 1H) ppm; ¹³C NMR (125 MHz, CDCl₃): δ 170.8, 160.0, 149.5, 149.4, 149.3, 148.1, 143.0, 130.0, 129.2, 124.9, 124.4, 122.0, 119.4, 117.2, 114.6, 113.6, 111.6, 104.1, 103.6, 103.5, 101.6, 56.2, 56.1, 56.0, 55.7, 55.0, 39.2 (2C) ppm; HRMS (ESI): *m/z* calcd for C₂₈H₂₇NO₆ 474.1911, found 474.1914 [M+H]⁺.

4.1.1.13 4-(3,4-Difluorophenyl)-6,7,10,11-tetramethoxy-3,4-dihydrodibenzo[f,h]quinolin-2(1H)-one (8m)

Off white solid, yield 87%; mp: 290–292 °C; ¹H NMR (500 MHz, CDCl₃): δ 9.64 (s, 1H), 7.84 (s, 1H), 7.80 (s, 1H), 7.48 (s, 1H), 7.05 (s, 1H), 7.01 (t, *J* = 9.46 Hz, 1H), 6.94–6.89 (m, 2H), 4.87 (d, *J* = 7.01 Hz, 1H), 4.14 (s, 3H), 4.09 (s, 3H), 4.04 (s, 3H), 3.86 (s, 3H), 3.32–3.27 (m, 1H), 2.94 (d, *J* = 15.86 Hz, 1H) ppm; ¹³C NMR (125 MHz, CDCl₃): δ 170.2, 149.7, 149.6, 149.5, 148.3, 138.2 (q, *J*_{C-F} = 4.5 Hz), 129.3, 125.1, 123.9 (d, *J*_{C-F} = 236.1 Hz), 123.0 (q, *J*_{C-F} = 3.6 Hz), 122.1, 117.9, 117.7, 117.1, 116.2, 116.1, 113.7, 103.8, 103.7, 103.6, 101.6, 56.3, 56.2, 56.1, 55.7, 39.2, 38.3 ppm; HRMS (ESI): *m/z* calcd for C₂₇H₂₃F₂NO₅ 480.1617, found 480.1622 [M+H]⁺.

4.1.1.14 6,7,10,11-Tetramethoxy-4-(3-methylthiophen-2-yl)-3,4-dihydrodibenzo[f,h]quinolin-

2(1H)-one (8n)

Light brown solid, yield 90%; mp: >300 °C; ¹H NMR (500 MHz, CDCl₃): δ 9.65 (s, 1H), 7.83 (s, 1H), 7.78 (s, 1H), 7.49 (s, 1H), 7.10 (s, 1H), 6.88 (d, *J* = 5.03 Hz, 1H), 6.80 (d, *J* = 5.03 Hz, 1H), 5.17 (d, *J* = 6.86 Hz, 1H), 4.13 (s, 3H), 4.07 (s, 3H), 4.03 (s, 3H), 3.90 (s, 3H), 3.28–3.24 (m, 1H), 2.91 (d, *J* = 15.56 Hz, 1H), 2.45 (s, 3H) ppm; ¹³C NMR (125 MHz, CDCl₃): δ 170.3, 149.5, 149.3 (2C), 148.1, 138.9, 131.8, 130.0, 128.9, 126.9, 125.0, 123.9, 122.9, 121.9, 117.2, 115.5, 103.6, 103.5, 101.7, 56.2 (2C), 56.0, 55.5, 38.6, 33.1, 13.7 ppm; HRMS (ESI): *m/z* calcd for C₂₆H₂₅NO₅S 464.1526, found 464.1522 [M+H]⁺.

4.1.1.15 6,7,10,11-Tetramethoxy-4-(thiophen-2-yl)-3,4-dihydrodibenzo[f,h]quinolin-2(1H)-one (8o)

Off white solid, yield 92%; mp: >300 °C; ¹H NMR (500 MHz, CDCl₃): δ 9.80 (s, 1H), 7.83 (s, 1H), 7.81 (s, 1H), 7.53 (s, 1H), 7.30 (s, 1H), 7.08 (d, *J* = 5.03 Hz, 1H), 6.78 (t, *J* = 3.96 Hz, 1H), 6.73 (d, *J* = 3.20 Hz, 1H), 5.14 (d, *J* = 6.40 Hz, 1H), 4.13 (s, 3H), 4.10 (s, 3H), 4.07 (s, 3H), 3.95 (s, 3H), 3.29–3.25 (m, 1H), 3.11 (d, *J* = 15.71 Hz, 1H) ppm; ¹³C NMR (125 MHz, CDCl₃): δ 170.6, 149.6, 149.5, 149.4, 148.1, 144.6, 128.7, 127.0, 124.9, 124.6, 124.3, 123.9, 121.9, 117.2, 115.3, 103.9, 103.6, 103.4, 101.6, 56.2, 56.1, 56.0, 55.8, 39.3, 34.4 ppm; HRMS (ESI): *m/z* calcd for C₂₅H₂₃NO₅S 450.1370, found 450.1365 [M+H]⁺.

4.1.1.16 4-(Benzo[d][1,3]dioxol-5-yl)-6,7,10,11-tetramethoxy-3,4-dihydrodibenzo[f,h]quinolin-2(1H)-one (8p)

Light brown solid, yield 80%; mp: 284–286 °C; ¹H NMR (500 MHz, CDCl₃): δ 9.84 (s, 1H), 7.83 (s, 1H), 7.79 (s, 1H), 7.52 (s, 1H), 7.14 (s, 1H), 6.65 (s, 2H), 6.61 (s, 1H), 5.83 (d, *J* = 4.42 Hz, 2H), 4.82 (d, *J* = 7.17 Hz, 1H), 4.13 (s, 3H), 4.08 (s, 3H), 4.02 (s, 3H), 3.88 (s, 3H), 3.29–3.25 (m, 1H), 2.92 (d, *J* = 15.56 Hz, 1H) ppm; ¹³C NMR (125 MHz, CDCl₃): δ 170.9, 149.4, 149.3, 149.2, 149.1, 148.0, 146.5, 135.2, 129.4, 124.8, 124.2, 121.9, 120.1, 117.3, 114.7, 108.6, 107.4, 104.0, 103.5, 103.4, 101.9, 100.9, 56.2, 56.1, 56.0, 55.7, 39.6, 38.9 ppm; HRMS (ESI): *m/z* calcd for C₂₈H₂₅NO₇ 488.1704, found 488.1705 [M+H]⁺.

4.1.1.17 4-(2,3-Dihydrobenzo[b][1,4]dioxin-6-yl)-6,7,10,11-tetramethoxy-3,4-dihydrodibenzo[f,h]quinolin-2(1H)-one (8q)

Light brown solid, yield 80%; mp: 287–289 °C; ¹H NMR (500 MHz, DMSO-*d*₆): δ 10.27 (s, 1H), 7.84–7.80 (m, 3H), 7.71 (t, *J* = 4.42 Hz, 1H), 7.14–7.11 (m, 1H), 6.65–6.59 (m, 1H),

6.52–6.50 (m, 1H), 4.74 (d, $J = 5.95$ Hz, 1H), 4.09–4.07 (m, 3H), 4.05 (d, $J = 5.79$ Hz, 3H), 3.99 (t, $J = 6.25$ Hz, 6H), 3.80–3.77 (m, 3H), 3.11–3.06 (m, 2H), 2.73–2.69 (m, 1H) ppm; ^{13}C NMR (125 MHz, DMSO- d_6): δ 169.5, 149.0, 148.8, 148.6, 147.5, 143.1, 142.0, 135.4, 129.7, 124.3, 123.8, 121.1, 119.7, 117.0, 116.9, 115.4, 114.7, 104.5, 104.3, 104.1, 103.1, 63.9, 63.8, 55.9, 55.8, 55.7, 55.2, 38.9, 37.0 ppm; HRMS (ESI): m/z calcd for $\text{C}_{29}\text{H}_{27}\text{NO}_7$ 502.1860, found 502.1856 $[\text{M}+\text{H}]^+$.

4.1.1.18 *6,7,10,11-Tetramethoxy-4-(naphthalen-1-yl)-3,4-dihydrodibenzo[*f,h*]quinolin-2(1*H*)-one (8r)*

Yellow solid, yield 78%; mp: >300 °C; ^1H NMR (500 MHz, $\text{CDCl}_3+\text{DMSO}-d_6$): δ 10.00 (s, 1H), 8.43 (d, $J = 8.39$ Hz, 1H), 7.94 (d, $J = 7.93$ Hz, 1H), 7.87 (s, 1H), 7.79 (s, 1H), 7.70 (t, $J = 7.78$ Hz, 3H), 7.58 (t, $J = 7.47$ Hz, 1H), 7.14 (t, $J = 7.62$ Hz, 1H), 6.96–6.94 (m, 2H), 5.71 (d, $J = 7.62$ Hz, 1H), 4.15 (s, 3H), 4.05 (d, $J = 4.27$ Hz, 6H), 3.48–3.36 (m, 5H) ppm; ^{13}C NMR (125 MHz, $\text{CDCl}_3+\text{DMSO}-d_6$): δ 169.3, 149.1, 148.7, 148.6, 147.5, 137.2, 133.8, 130.8, 130.0, 129.0, 127.3, 126.7, 125.7, 125.4, 124.4, 124.0, 123.8, 122.6, 121.3, 117.0, 114.4, 104.5, 104.2, 104.1, 103.2, 55.9, 55.8 (2C), 54.6, 38.0, 33.7 ppm; HRMS (ESI): m/z calcd for $\text{C}_{31}\text{H}_{27}\text{NO}_5$ 494.1962, found 494.1964 $[\text{M}+\text{H}]^+$.

4.2 Biology

4.2.1. Cell Cultures

Cells were procured from National Centre for Cell Science (NCCS) Pune, India and stocks were maintained under sterile conditions. lung (A549), prostate (PC-3 and DU145), breast (MCF-7) and colon (HT 29 and HCT-116) cancer cells were grown in tissue culture flasks in DMEM (Dulbecco modified Eagle medium, Sigma), MEM (Minimum Essential Medium, Sigma) or RPMI 1640 medium, Sigma, supplemented with 10% fetal bovine serum with 1X stabilized antibiotic-antimycotic solution (Sigma) in a CO_2 incubator at 37 °C with 5% CO_2 and 90% relative humidity.

4.2.2 In vitro cytotoxic activity

MTT assay was performed to determine the cytotoxicity for all the new compounds **8a-r**. 1×10^4 cells per well were seeded in 100 μL respective media, supplemented with 10% FBS in each well of 96-well microculture plates and incubated at 37 °C for 24 h, in a CO_2 incubator. Samples were diluted to the required concentrations in culture medium, were added to the

wells with respective vehicle control. After incubating for 48 h, 100 μ L MTT (3-(4,5-dimethylthiazol-2-yl)-2,5-diphenyl tetrazolium bromide) (0.5 mg/mL) was added to all the plates and allowed for 4 h incubation. Then, the supernatant was carefully decanted from each well, formazon crystals were dissolved in 200 μ L of DMSO and at 570 nm wavelength absorbance was recorded.

4.2.3 DAPI nuclear staining

DAPI staining was performed to observe morphological changes in nucleus. After treatment of A549 cells with **8p** for 48 h, cells were washed with PBS and solubilized with 0.1% Tween 20 for 10 min followed by staining with 1 μ M DAPI. Control and treated cells were observed with fluorescence microscope (Model: Nikon, Japan) with excitation at 359 nm and emission at 461 nm using DAPI filter at 200X magnification.

4.2.4 Acridine orange–ethidium bromide (AO–EB) staining

A549 cells were plated at a concentration of 1×10^6 cell/ml and treated with different concentrations of compound **8p**. Plates were incubated at 37 °C in an atmosphere of 5% CO₂ for 48 h. 10 μ L of fluorescent dyes containing Acridine Orange (AO) and Ethidium Bromide (EB) added into each well in equal volumes (10 μ g/mL) respectively and after 10 min the cells were visualized under fluorescence microscope (Nikon, Inc. Japan) with excitation (488 nm) and emission (550 nm) at 200x magnification.

4.2.5 Morphological studies

A549 cells with a density of 1×10^5 cells/mL were plated in 6 well culture plates and allowed to adhere for overnight. Cells were incubated with various concentrations of **8p**. After 48 h, cells were observed for morphological changes and images were captured by using phase contrast microscope (Nikon).

4.2.6 Effect on reactive oxygen species (ROS)

A549 cells with a density of (1×10^6 cells/mL) were plated in 24 well plates and allowed to adhere for overnight. Then the cells were treated with 1.25, 2.5, 5.0 and 10.0 μ M compound **8p** for 24 h. The media was replaced with culture medium containing DCFDA dye (10 μ M) and incubated in dark for 30 min. The intensity of fluorescence from samples was determined

by multimode plate reader at an excitation and emission wavelength of 488 and 525 nm, respectively and the images were captured by fluorescent microscope.

4.2.7 Analysis of mitochondrial membrane potential ($\Delta\Psi_m$)

A549 cells (1×10^6 cells/mL) were plated in 6 well plates and allowed to adhere for overnight. The cells were incubated with 1.25, 2.5, 5.0 and 10 μ M concentrations of **8p** for 24 h. cells were collected, washed with PBS and resuspended in solution of JC-1 (2.5 μ g/mL) and allowed for incubation at 37 °C for 10 min. The cells were washed twice with PBS and cells were trypsinized, centrifuged and analyzed by flow cytometer (BD FACSVerse™, USA).

4.2.8 Annexin V/Propidium iodide dual staining assay

The Annexin V/Propidium iodide dual staining assay was performed using A549 cells. To quantify the percentage of apoptotic cells, A549 cells (1×10^6 mL per well) were plated in six-well culture plates and allowed to grow for 24 h. After treatment with the compound **8p** (2.5, 5.0 and 10 μ M) for 48 h, cells were collected by trypsinisation. The collected cells were washed twice with ice-cold PBS, then incubated with 200 μ L 1 x binding buffer containing 5 μ L Annexin V-Alexa flour 488, and then in 300 μ L 1 x binding buffer containing 5 μ L Propidium iodide (PI) for 15 min at room temp in the dark. After incubation, cells were analyzed for apoptosis using flow-cytometer.

4.2.9 Cell cycle analysis

The accumulation of cells in various phases of cell cycle was analysed by Flow cytometric analysis (FACS). A549 cells were incubated with **8p** at different concentrations 1.25, 2.5, 5.0, and 10 μ M for 48 h. control and **8p** treated cells were harvested, washed with PBS, fixed in 70% ethanol and stained with propidium iodide (50 μ g/mL sigma aldrich) in the presence of RNase A (20 μ g/mL) containing 0.1% Triton X-100 at 37°C for 30 min in dark, and about 10000 events were analyzed by flow cytometer.

4.2.10 Effect on tubulin polymerization

Tubulin polymerization kit was procured from Cytoskeleton, Inc. (BK011). To study the effect of compound **8p**, fluorescence based *in vitro* tubulin polymerization assay was

performed following the manufacturer's protocol. The reaction mixture having porcine brain tissue (2 mg/mL) in 80 mM PIPES at pH 6.9, 2.0 mM MgCl₂, 0.5 mM EGTA, 1.0 mM GTP and glycerol in the presence and absence of test compound **8p** (final concentration of 10 μ M) was prepared and added to each well of 96-well plate. Tubulin polymerization was followed by a time dependent increase in fluorescence due to the insertion of a fluorescence reporter into microtubules as polymerization takes place. Spectramax M4 Multi mode Micro plate Detection System was used to measure Fluorescence emission at 440 nm (excitation wavelength is 360 nm). podophyllotoxin was used as positive control in the assay at 5 μ M final concentration. The IC₅₀ value was calculated from the drug concentration required for inhibiting 50% of tubulin assembly compared to control.

4.2.11 Molecular docking

The crystal co-ordinates of α,β -tubulin subunits were retrieved from the protein data bank (PDB ID: 1SA1). The 3D structure of compound **8p** was drawn on Maestro Molecule Builder of Schrödinger. The molecule was optimised using OPLS_2005 force field in LigPrep module of Schrödinger. Docking procedure was performed according to the standard protocol implemented in maestro software, version 9.9 and the compound **8p** was docked into the α,β -tubulin interphase. The ligand –protein complex was analysed for interactions and 3D pose of most active compound **8p** was imaged using Schrödinger and PyMOL v0.99.

Acknowledgements

Authors are thankful to DoP, Ministry of Chemicals & Fertilizers, Govt. of India, New Delhi, for the award of NIPER fellowship. Dr. N. Shankaraiah thankful to SERB, DST, Govt. of India for the start-up grant (YSS-2015-001709).

5.0 References

1. M. Center, R. Siegel, A. Jemal, Atlanta: American Cancer Society. (2011) 1–52.
2. S. Raguz, E. Yague, Br. J. Cancer. 99 (2008) 387–391; (b) A. Kamal, S. Nekkanti, N. Shankaraiah, M. Satish, Springer International Publishing. (2017) 609–629.
3. M.S. Ricci, W.-X. Zong, Oncologist. 11 (2006) 342–357; (b) S. Nekkanti, R. Tokala, N. Shankaraiah, Curr. Med. Chem. 24 (2017) 2887–2907.
4. F.E. Koehn, G.T. Carter, Nat. Rev. Drug Discovery. 4 (2005) 206–220; (b) L. Yang, L.H. Qin, S.A. Bligh, A. Bashall, C.F. Zhang, M. Zhang, Z.T. Wang, L.S. Xu, Bioorg.

- Med. Chem. 14 (2006) 3496–3501; (c) A. Stoye, T.E. Peez, T. Opatz, J. Nat. Prod. 76 (2013) 275–278.
5. M. Deng, B. Su, H. Zhang, Y. Liu, Q. Wang, RSC Advances. 4 (2014) 14979–14984.
 6. (a) L. Wei, A. Brossi, R. Kendall, K.F. Bastow, S.L. Morris-Natschke, Q. Shi, K.H. Lee, Bioorg. Med. Chem. 14 (2006) 6560–6569; (b) T. Ikeda, T. Yaegashi, T. Matsuzaki, R. Yamazaki, S. Hashimoto, S. Sawada, Bioorg. Med. Chem. Lett. 21 (2011) 5978–5981.
 7. (a) L. Yang, L.H. Qin, S.A. Bligh, A. Bashall, C.F. Zhang, M. Zhang, Z.T. Wang, L.S. Xu, Bioorg. Med. Chem. 14 (2006) 3496–3501; (b) C.W. Yang, W. L. Chen, P. L. Wu, H. Y. Tseng, S.J. Lee, Mol Pharmacol, 69 (2006) 749–758.
 8. J.Y. Choi, W. Gao, J. Odegard, H.S. Shiah, M. Kashgarian, J.M. McNiff, D. C. Baker, Y.C. Cheng, J. Craft, Arthritis & Rheumatism. 54 (2006) 3277–3283.
 9. M.G. Banwell, A. Bezos, C. Burns, I. Kruszelnicki, C.R. Parish, S. Su, M. O. Sydnese, Bioorg. Med. Chem. Lett. 16 (2006) 181–185.
 10. X. You, M. Pan, W. Gao, H. S. Shiah, J. Tao, D. Zhang, F. Koumpouras, S. Wang, H. Zhao, J.A. Madri, Arthritis & Rheumatism, 54 (2006) 877–886.
 11. H. M. Faidallah, K.A. Shaikh, T.R. Sobahi, K.A. Khan, A.M. Asiri, Molecules, 18 (2013) 15704–15716.
 12. B. Su, C. Cai, M. Deng, D. Liang, L. Wang, Q. Wang, Bioorg. Med. Chem. Lett. 24 (2014) 2881–2884.
 13. B. Baumgartner, C.A. Erdelmeier, A.D. Wright, T. Rali, O. Sticher, Phytochemistry. 29 (1990) 3327–3330.
 14. (a) Z. Wang, M. Wu, Y. Wang, Z. Li, L. Wang, G. Han, F. Chen, Y. Liu, K. Wang, A. Zhang, L. Meng, Q. Wang, Eur. J. Med. Chem. 51 (2012) 250–258; (b) Y-Z. Lee, C-W. Yang, H-Y. Hsu, Y-Q. Qiu, T-K. Yeh, H-Y. Chang, Y-S. Chao, S-J. Lee, J. Med. Chem. 55 (2012) 1036–10377; (c) X. Yang, Q. Shi, C-Y. Lai, C-Y. Chen, E. Ohkoshi, S-C. Yang, C-Y. Wang, K.F. Bastow, T-S. Wu, S-L. Pan, C-M. Teng, P-C. Yang, K-H. Lee, J. Med. Chem. 55 (2012) 6751–6761.
 15. (a) J.C. Lin, S.C. Yang, T.M. Hong, S.L. Yu, Q. Shi, L. Wei, H.Y. Chen, P.C. Yang, K.H. Lee, J. Med. Chem. 52 (2009) 1903–1911; (b) B. Su, F. Chen, Q. Wang, J. Med. Chem. 78 (2013) 2775–2779.
 16. X. Yang, Q. Shi, S.C. Yang, C.Y. Chen, S.L. Yu, K.F. Bastow, S.L. Morris Natschke, P.C. Wu, C.Y. Lai, T. S. Wu, J. Med. Chem. 54 (2011) 5097–5107.

17. (a) M.A. Shareef, D. Duscharla, G. Ramasatyaveni, N.R. Dhoke, A. Das, R. Ummanni, A. K. Srivastava, *Eur. J. Med. Chem.* 89 (2015) 128–137; (b) D. Passarella, B. Peretto, R. B. Yepes, G. Cappelletti, D. Cartelli, C. Ronchi, J. Snaith, G. Fontana, B. Danieli, J. Borlak, *Eur. J. Med. Chem.* 45 (2010) 219–226; (c) L. Zhang, Z. Zhang, J. Wang, Y. Chen, F. Chen, Y. Lin, X. Zhu, *RSC Advances*, 6 (2016) 2895–2903.
18. M. Duca, D. Guianvarch, P. Meresse, E. Bertounesque, D. Dauzonne, L.K. Berthier, S. Thiot, S. Léonce, A. Pierre, B. Pfeiffer, *J. Med. Chem.* 48 (2005) 593–603.
19. (a) V.V. Semenov, B.V. Lichitsky, A.N. Komogortsev, A.A. Dudinov, M.M. Krayushkin, L.D. Konyushkin, O.P. Atamanenko, I.B. Karmanova, Y.A. Strelenko, B. Shor, M.N. Semenova, A.S. Kiselyov, *Eur. J. Med. Chem.* 125 (2017) 573–585; (b) I.V. Magedov, L. Frolova, M. Manpadi, U.D. Bhoga, H. Tang, N.M. Evdokimov, O. George, K.H. Georgiou, S. Renner, M.U. Getlik, *J. Med. Chem.* 54 (2011) 4234–4246; (c) Y. Hitotsuyanagi, M. Fukuyo, K. Tsuda, M. Kobayashi, A. Ozeki, H. Itokawa, K. Takeya, *Bioorg. Med. Chem. Lett.* 10 (2000) 315–317.
20. (a) N. Jeedimalla, M. Flint, L. Smith, A. Haces, D. Minond, S.P. Roche, *Eur. J. Med. Chem.* 106 (2015) 167–179; (b) C-L. Shi, H. Chen, D-Q. Shi, *J. Heterocyclic Chem.* 48 (2011) 351–354; (c) X. Zhong, G. Dou, D. Wang, *Molecules*, 18 (2013) 13139–13147; (d) S. Nekkanti, K. Veeramani, S.S. Kumari, N. Shankaraiah, *RSC Adv.* 6 (2016) 103556–103566; (e) P. Sharma, N. P. Kumar, N. H. Krishna, D. Prasanna, B. Sridhar, N. Shankaraiah, *Org. Chem. Front.* 3 (2016) 1503–1508.
21. M.N. Semenova, A.S. Kiselyov, D.V. Tsyganov, L.D. Konyushkin, S.I. Firgang, R.V. Semenov, O.R. Malyshev, M. M. Raihstat, F. Fuchs, A. Stielow, *J. Med. Chem.* 54 (2011) 7138–7149.
22. (a) S. Kandil, J.M. Wymant, B.M. Kariuki, A.T. Jones, C. McGuigan, A.D. Westwell, *Eur. J. Med. Chem.* 110 (2016) 311–325; (b) A. Kamal, T.S. Reddy, S. Polepalli, S. Paidakula, V. Srinivasulu, V.G. Reddy, N. Jain, N. Shankaraiah, *Bioorg. Med. Chem. Lett.* 24 (2014) 3356–3360.
23. N. Shankaraiah, N.P. Kumar, S.B. Amula, S. Nekkanti, M.K. Jeengar, V.G.M. Naidu, T.S. Reddy, A. Kamal, *Bioorg. Med. Chem. Lett.* 25 (2015) 4239–4244; (b) A. Kamal, T.S. Reddy, S. Polepalli, N. Shalini, V.G. Reddy, A.V.S. Rao, N. Jain, N. Shankaraiah, *Bioorg. Med. Chem.* 22 (2014) 5466–5475.

24. N. Ma, B. Jiang, G. Zhang, S-J. Tu, W. Wever, G. Li, *Green. Chem.* 12 (2010) 1357–1361.
25. N.P. Kumar, P. Sharma, T.S. Reddy, S. Nekkanti, N. Shankaraiah, G. Lalita, S. Sujanakumari, S.K. Bhargava, V.G. M. Naidu, A. Kamal, *Eur. J. Med. Chem.* 127 (2017) 305–317.
26. (a) K. Wang, Y. Hu, M. Wu, Z. Li, Z. Liu, B. Su, A. Yu, Y. Liu, Q. Wang, *Tetrahedron.* 66 (2010) 9135–9140; (b) Y.Z. Lee, C.W. Yang, H.Y. Hsu, Y.Q. Qiu, T.K. Yeh, H.Y. Chang, Y.S. Chao, S.J. Lee, *J. Med. Chem.* 55 (2012) 10363–10377; (c) T.R. Govindachari, M. Lakshmikantham, K. Nagarajan, B. Pai, *Tetrahedron.* 4 (1958) 311–324.
27. (a) T. Mosmann, *J. Immunol. Meth.* 65 (1983) 55–63; (b) P. Sharma, K.R. Senwar, M.K. Jeengar, T.S. Reddy, V.G.M. Naidu, A. Kamal, N. Shankaraiah, *Eur. J. Med. Chem.* 104 (2015) 11–24.
28. B.I. Tarnowski, F.G. Spinale, J.H. Nicholson, *Biotech Histochem.* 66 (1991) 297–302.
29. P. Sharma, D. Thummuri, T.S. Reddy, K.R. Senwar, V.G.M. Naidu, G. Srinivasulu, S.K. Bhargava, N. Shankaraiah, *Eur. J. Med. Chem.* 122 (2016) 584–600; (b) K.R. Senwar, P. Sharma, T.S. Reddy, M.K. Jeengar, V.L. Nayak, V.G.M. Naidu, A. Kamal, N. Shankaraiah, *Eur. J. Med. Chem.* 102 (2015) 413–424.
30. E. Eruslanov, S. Kusmartsev, *Methods. Mol. Biol.* 594 (2010) 57–72.
31. N. Kulabas, E. Tatar, O.B. Ozakpinar, D. Ozsavci, C. Pannecouque, E.D. Clercq, I. Kucukguzel, *Eur. J. Med. Chem.* 121 (2016) 58–70.
32. T.S. Reddy, V.G. Reddy, H. Kulhari, R. Shukla, A. Kamal, V. Bansal, *Eur. J. Med. Chem.* 117 (2016) 157–166.
33. N. Shankaraiah, S. Nekkanti, U.R. Brahma, N.P. Kumar, N. Deshpande, D. Prasanna, K.R. Senwar, U.J. Lakshmi, *Bioorg. Med. Chem.* 25 (2017) 4805–4816.
34. R.B Ravelli, B. Gigant, P.A Curmi, I. Jourdain, S. Lachkar, A. Sobel, M. Knossow, *Nature* 428 (2004) 198–202.

Research Highlights

- Sulfamic acid promoted synthesis of phenanthrene fused-dihydrodibenzo-quinolinones.
- Cytotoxicity on selected cancer cell lines and apoptosis inducing studies.
- In A549 lung cancer cells, **8p** caused the collapse of $D\Psi m$ and enhanced ROS.
- Compound **8p** induced dose dependent G2/M and Sub G1 cell cycle arrest in A549 cells.
- **8p** Inhibited the tubulin polymerization and thereby prevents cancer cell division.

Graphical Abstract

Sulfamic acid promoted one-pot synthesis of phenanthrene fused-dihydrodibenzo-quinolinones: Anticancer activity, tubulin polymerization inhibition and apoptosis inducing studies

Niggula Praveen Kumar,^a Sowjanya Thatikonda,^c Ramya Tokala,^a S. Sujana Kumari,^b Uppu Jaya Lakshmi,^b Chandraiah Godugu,^{*c} Nagula Shankaraiah,^{a*} Ahmed Kamal^{a*}

^aDepartment of Medicinal Chemistry, ^bDepartment of Pharmacology and Toxicology, ^cDepartment of Regulatory Toxicology, National Institute of Pharmaceutical Education and Research (NIPER), Hyderabad 500 037, India

Graphical abstract

